

A new model of composite interstellar dust grains

N.V. Voshchinnikov^{1,2}, V.B. Il'in^{1,2}, Th. Henning³, and D.N. Dubkova¹

¹ Sobolev Astronomical Institute, St. Petersburg University, Universitetskii prosp. 28, St. Petersburg, 198504 Russia

² Isaac Newton Institute of Chile, St. Petersburg Branch

³ Max-Planck-Institut für Astronomie, Königstuhl 17, D-69117 Heidelberg, Germany

Received <date>; accepted <date>

Abstract. The approach to model composite interstellar dust grains, using the exact solution to the light scattering problem for multi-layered spheres as suggested by Voshchinnikov & Mathis (1999), is further developed. Heterogeneous scatterers are represented by particles with very large number of shells, each including a homogeneous layer per material considered (amorphous carbon, astronomical silicate and vacuum). It is demonstrated that the scattering characteristics (cross-sections, albedo, asymmetry factor, etc.) well converge with the increase of the number of shells (layers) and each of the characteristics has the same limit independent of the layer order in the shells. The limit obviously corresponds to composite particles consisting of several well mixed materials. However, our results indicate that layered particles with even a few shells (layers) have characteristics close enough to these limits. The applicability of the effective medium theory (EMT) mostly utilized earlier to approximate inhomogeneous interstellar grains is examined on the basis of the new model. It is shown that the EMT rules generally have an accuracy of several percent in the whole range of particle sizes provided the porosity does not exceed about 50%. For larger porosity, the EMT rules give wrong results. Using the model, we reanalyze various basic features of cosmic dust — interstellar extinction, scattered radiation, infrared radiation, radiation pressure, etc. It is found that an increase of porosity typically leads to an increase of cross-sections, albedo and the sweeping efficiency of small grains as well as to a decrease of dust temperature and the strength of infrared bands (the EMT fails to produce these effects). As an example of the potential of the model, it is applied to reproduce the extinction curves in the directions to ζ Oph and σ Sco using subsolar cosmic abundances. We also conclude that metallic iron even in negligible amount ($\lesssim 1\%$ by the volume fraction) is unlikely to form a layer on or inside a grain because of peculiar absorption of radiation by such particles.

Key words. Polarization – Scattering – circumstellar matter – Stars: individual: ζ Oph, σ Sco – ISM: clouds – dust, extinction – Comets

1. Introduction

Scientists felt the necessity to treat the scattering by composite and inhomogeneous particles and media (i.e., consisting of several components) essentially earlier than the existence of interstellar dust has been generally established. It was started by Garnett (1904) who found the averaged or effective dielectric functions of a medium assuming that one material was a matrix (host material) in which the other material was embedded (so called Maxwell–Garnett mixing rule of Effective Medium Theory; EMT). When the roles of the inclusion and the host material are reversed, the inverse Garnett rule is obtained. Later, Bruggeman (1935) deduced another rule which was symmetric with respect to the interchange of

materials. These classical mixing rules are the most popular ones till now.

Many scientific and applied problems require exact calculations of light scattering by inhomogeneous particles. This became first possible in the beginning of the 1950s when the Mie solution for homogeneous spheres was generalized to core-mantle spherical particles in three independent papers (Aden & Kerker 1951, Shifrin 1952, Güttler 1952). Güttler's solution was used by Wickramasinghe (1963) who first calculated the extinction of graphite core-ice mantle grains. Such particles should be formed in interstellar clouds where the bare particles ejected from stellar atmospheres may accumulate mantles from volatile elements.

An unsuccessful first attempt to detect the $3.1\,\mu\text{m}$ feature of solid H_2O together with pioneering experiments on the ultraviolet (UV) photoprocessing of mixtures of volatile molecules stimulated Greenberg (1984) to suggest

the idea of the formation of complex organic molecules on silicate cores. In dense clouds, an additional layer of photolysed volatile ices appears due to accretion, so the particles become three-layered. Further, the grains around protostellar objects are covered by a layer of unphotolysed accumulated atoms and molecules, then the particles become four-layered. This core-mantle model was modified several times by Greenberg and his co-workers (Hong & Greenberg 1980, Greenberg & Li 1996, Li & Greenberg 1997, see also a brief history of development of dust models in Li & Greenberg 2002). Another model of inhomogeneous interstellar grains was proposed by Duley et al. (1989) who considered silicate grains coated by thin layers of hydrogenated amorphous carbon (HAC) and amorphous carbon. Although the possible origin of such grains remains unclear, they were applied to the explanation of interstellar extinction, extended red emission, unidentified infrared (IR) bands, etc. Jones et al. (1990) showed that the evolution of HAC mantle in the interstellar conditions could result in the appearance of a layer of polymeric HAC overlaying the graphitic HAC which in its turn covered the silicate core. However, the optical properties of three and more layered particles were never calculated exactly: usually some EMT or, in the best case, a core-mantle grain model was used.

Core-mantle (or even multi-layered) grains are possibly produced in the atmospheres of late-type stars. McCabe (1982) suggested that because of the inverse greenhouse effect silicon carbide core-graphite mantle grains could be produced in carbon stars. This idea was further developed by Kozasa et al. (1996) who demonstrated that nucleation of SiC grains always preceded that of carbon grains if the difference between the temperature of gas and small clusters was taken into account. The application of this model to interpretation of the spectral energy distribution of carbon stars show that the core-mantle grains better fit the data for dust envelopes of evolved stars than the mixtures of homogeneous grains which are able to reproduce the data for optically thin envelopes (Lorenz-Martins et al. 2001).

Mathis & Whiffen (1989) introduced the model of composite grains which were very porous (the volume fraction of vacuum $\sim 80\%$) aggregates of small amorphous carbon, silicate and iron particles. The optical properties of such particles were calculated with the Mie theory and EMT. Mathis (1996) updated the composite grain model taking into account new subsolar abundances of heavy elements. The new model consisted of three components where the visual/near-IR extinction was explained by aggregates with $\sim 45\%$ vacuum in volume.

Now light scattering computations for inhomogeneous (composite) particles with layers or inclusions from different materials or aggregate particles can be made using the discrete dipole approximation (DDA), the T-matrix method (TMM) or a simpler theory like the Mie theory for n -layered spheres (see Voshchinnikov 2002 for discussion). However, calculations with the DDA are very time-consuming and at the present can be used rather for il-

lustrative than mass calculations (e.g., Wolff et al. 1994, Vaidya et al. 2001). The idea of composite particles as multi-layered spheres (Voshchinnikov & Mathis 1999, see also Iatì et al. 2001) looks a bit artificial but attractive from the point of view of numerical realization. Such a model permits to include an arbitrary fraction of any material and the computations require rather moderate resources.

In this paper, we develop the model of composite interstellar grains based on *exact* calculations for multi-layered spheres. The general description of the model is given in Sect. 2. We calculate different efficiency factors, albedo, etc. and analyze how they depend on the order and number of layers (Sect. 2.2) and the fraction of vacuum (Sect. 2.3). The possibility to describe the optical properties of multi-layered spheres using Mie theory with different EMT rules is considered in Sect. 3. The wavelength dependence of extinction by multi-layered particles is discussed in Sect. 4. The analysis of the radiation pressure on composite grains is presented in Sect. 5. The behaviour of albedo and asymmetry parameter as well as the intensity and polarization of the scattered radiation are studied in Sect. 6. The next section includes the consideration of grain temperature (Sect. 7.1), profiles of IR bands (Sect. 7.2), and grain opacities at $\lambda = 1$ mm (Sect. 7.3). Section 8 contains the application of the new model to the calculations of the extinction curves in the direction of two stars taking into account the subsolar cosmic abundances. We also analyze the possibility of pure iron to be a component of a multi-layered particle (Sect. 8.2). Concluding remarks are presented in Sect. 9.

Further development of the model will involve the consideration of non-spherical multi-layered grains based on the available light scattering methods (see Farafonov et al. 2003 for a review).

2. General description of the model

2.1. Basics

We construct composite grains as particles consisting of many concentric spherical layers of various materials, each with a specified volume fraction. Vacuum can be one of the materials, so a composite particle may have a central cavity or voids in the form of concentric layers. From the point of view of dust formation and growth, the presence of vacuum at the particle centre or in several voids distributed inside porous aggregate grain is rather natural while a particle with concentric spherical vacuum layers looks artificial. However, in the case of multi-layered composite spheres we can include at *any* position inside a particle *any* fraction of a material (from extremely small to very large) and produce the *exact* calculations. The latter is of particular importance for the consideration of very porous grains as suggested, for example, for comets (Greenberg & Hage 1991) or the disc of β Pictoris (Li & Greenberg 1998).

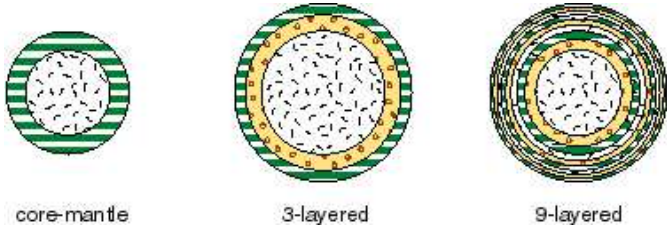


Fig. 1. The models of composite particles containing the same amount of two materials (carbon and silicate). The multi-layered spheres consist of an equal volume fraction (33.33%) of carbon, silicate and vacuum separated in equivolume spherical layers. The core-mantle particle has the same mass of carbon and silicate but is free of vacuum. As a result, its volume is less by $1/3$ and the outer radius is by $\sqrt[3]{1/3} \approx 0.69$ less.

The schematic representation of multi-layered spherical grains is given in Fig. 1. They are composed of a specified number of concentric spherical homogeneous layers. The amount of material is determined by its volume fraction V_i ($\sum_i V_i / V_{\text{total}} = 1$). The amount of vacuum (or the particle porosity \mathcal{P} , $0 \leq \mathcal{P} < 1$) can be introduced as

$$\mathcal{P} = V_{\text{vac}} / V_{\text{total}} = 1 - V_{\text{solid}} / V_{\text{total}}. \quad (1)$$

The order of the layers and their total number can be specified separately. Following Voshchinnikov & Mathis (1999, hereafter VM), we assume further that the concentric spherical layers of two or more different materials form a “shell”. The whole grain consists of a specified number of concentric shells, e.g. the simplest composite particle contains one shell of two materials (core-mantle or coated grain). As materials, we choose carbon and silicate which were used in many cosmic dust models (Mathis et al. 1977, Draine & Lee 1984). The illustrations of several composite grains are presented in Fig. 1. The core-mantle particle does not contain vacuum, but its mass is the same as that of the other two particles and, therefore, its outer radius is smaller. Note also that since the volume fractions are specified, the innermost layer is relatively thicker than the others.

The formal solution to the light scattering problem for multi-layered spheres can be easily written in matrix form (see, e.g., Kerker 1969). However, for practical reasons, it is better to use the recursive algorithm developed by Wu & Wang (1991) and Johnson (1996). In order to make calculations for highly absorbing particles of large size, several modifications were suggested by Wu et al. (1997) and Gurvich et al. (2001).

In our calculations presented below, composite particles of several materials are considered. The refractive indices for them were taken from the Jena–Petersburg Database of Optical Constants (JPDOC) which was described by Henning et al. (1999) and Jäger et al. (2003).

2.2. Dependence on the order and number of layers

The optical properties of core-mantle spheres have been studied rather well and seem to show no significant peculiarities (Prishivalko et al. 1984). In contrast, already three-layered spheres can produce anomalous extinction of light. This is illustrated in Fig. 2 where the extinction efficiency factors Q_{ext} are plotted for spheres consisting of 3, 9 and 18 equivolume layers. The layers are composed of amorphous carbon (AC1), astronomical silicate (astrosil) and vacuum, the volume fraction of each constituent is $1/3$. The optical constants for AC1 ($m = 1.98 + 0.23i$) and astrosil ($m = 1.68 + 0.03i$) correspond to the wavelength $\lambda = 0.55 \mu\text{m}$ and were taken from the papers of Rouleau & Martin (1991) and Laor & Draine (1993), respectively.

The order of the materials strongly affects the behaviour of extinction in the case of three-layered particles (the upper panel of Fig. 2). First of all, the position of vacuum (the core or the middle layer) is important. The curve for the case of particles with a carbon core and an outermost astrosil layer is the most peculiar curve. Here, a very rare situation is observed: The first maximum is damped, but there is a very broad second maximum which is the highest among the different cases. As follows from the upper panels of Figs. 3 and 4, the scattering efficiency depends stronger on the order of layers than the absorption efficiency. However, all the peculiarities disappear if the number of layers increases: The difference between the curves becomes rather small for particles with 9 layers (3 shells) and is hardly present for particles with 18 layers (6 shells; see the middle and lower panels of Figs. 2 – 7). This fact, noted by VM already, allows one to use *multi-layered particles as a new approximate model of composite grains*. Such a model is the *only* possible way to treat heterogeneous particles exactly when several materials are well mixed. Here the particle has to be divided in many shells ($\gtrsim 3 - 5$). Then we obtain a “composite” particle with “average” optical properties where the real order of materials in each shell can be ignored. For such particles, different efficiency factors as well as the particle albedo Λ and the asymmetry parameter g (or $\langle \cos \Theta \rangle$) depend on the volume fraction of materials only. Below we consider a particle consisting of 18 layers as a representative of a heterogeneous interstellar grain with well mixed constituents.

Solid thick lines at the lowest panels of Figs. 2 – 7 show the size dependence of the optical characteristics for compact ($\mathcal{P} = 0$) spheres consisting of the same amount of solid materials $V_{\text{solid}} / V_{\text{total}}$. To compare the optical properties of porous and compact particles, one needs to normalize the size parameter (or radius) of the compact (or porous) particle using the relation

$$x_{\text{porous}} = \frac{x_{\text{compact}}}{(1 - \mathcal{P})^{1/3}} = \frac{x_{\text{compact}}}{(V_{\text{solid}} / V_{\text{total}})^{1/3}}. \quad (2)$$

In the case of the particles presented in Figs. 2 – 7, this leads to stretching of the x scale for compact particles by a factor of $\sqrt[3]{3/2} \approx 1.145$. It can be seen that the presence of vacuum inside a composite particle reduces the

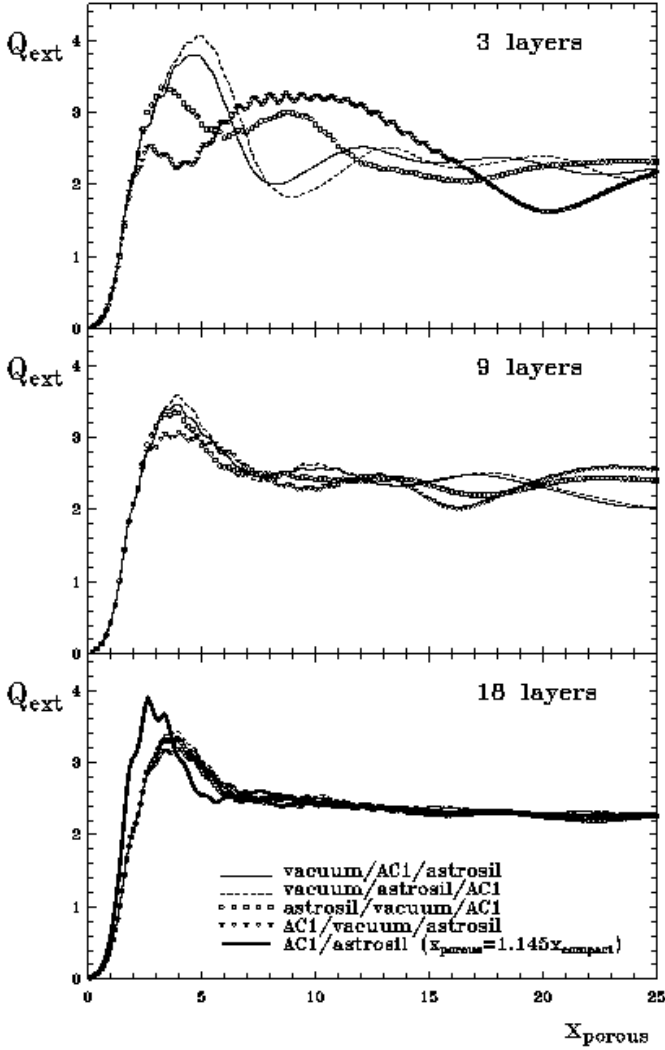


Fig. 2. Size dependence of the extinction efficiency factors for multi-layered spherical particles. The size parameter x_{porous} is calculated according to Eq. (2). Each particle contains an equal fraction (33.33%) of amorphous carbon (AC1), astrosil and vacuum separated in equivolume layers. The porosity of the particles with 3, 9 and 18 layers is the same ($\mathcal{P} = 1/3$). The cyclic order of the layers is indicated (starting from the core). The effect of the increase of the number of layers is illustrated. The thick line at the lowest panel corresponds to compact spheres consisting of AC1 and astrosil. For a given value of the size parameter, the compact and porous particles have the same mass. In order to reach that, the x scale for compact particles was stretched by a factor $\sqrt[3]{3/2} \approx 1.145$.

peak of the absorption efficiency (Fig. 4) and shifts that of the scattering efficiency (Fig. 3). Correspondingly, these two effects explain the behaviour of the curves for the extinction and radiation pressure factors (Figs. 2 and 5). A medium porosity influences the albedo and the asymmetry parameter only in a restricted range of the size parameters $x_{\text{porous}} \approx 3 - 10$ (see Figs. 6 and 7), but the properties

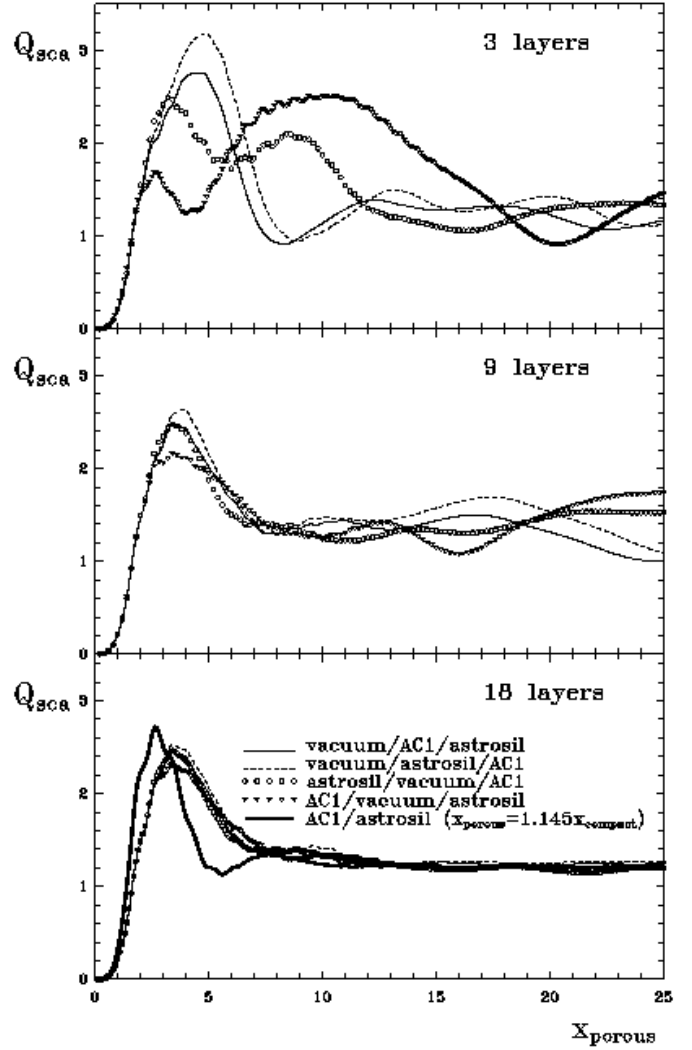


Fig. 3. The same as in Fig. 2 but now for scattering efficiency factors.

of very porous and compact particles of all sizes differ considerably (see discussion in the next Section).

2.3. Varying the fraction of vacuum

The fraction of vacuum in interstellar dust grains can be large. Very porous particles are often used to model cometary grains. For example, Greenberg & Hage (1991) indicate that the porosity of dust aggregates in comets can be in the range $0.93 < \mathcal{P} < 0.98$. Their conclusions are based on the model of porous grains developed by Hage & Greenberg (1990) who used for light scattering calculations the volume integral equation formulation method (a modification of DDA). The verification of this method was made in the case of small compact spheres but later the method was generalized to large and very porous particles. A qualitative agreement of the method with the Mie–Garnett calculations was found: in both cases the absorption efficiency cross-sections C_{abs} increase while the

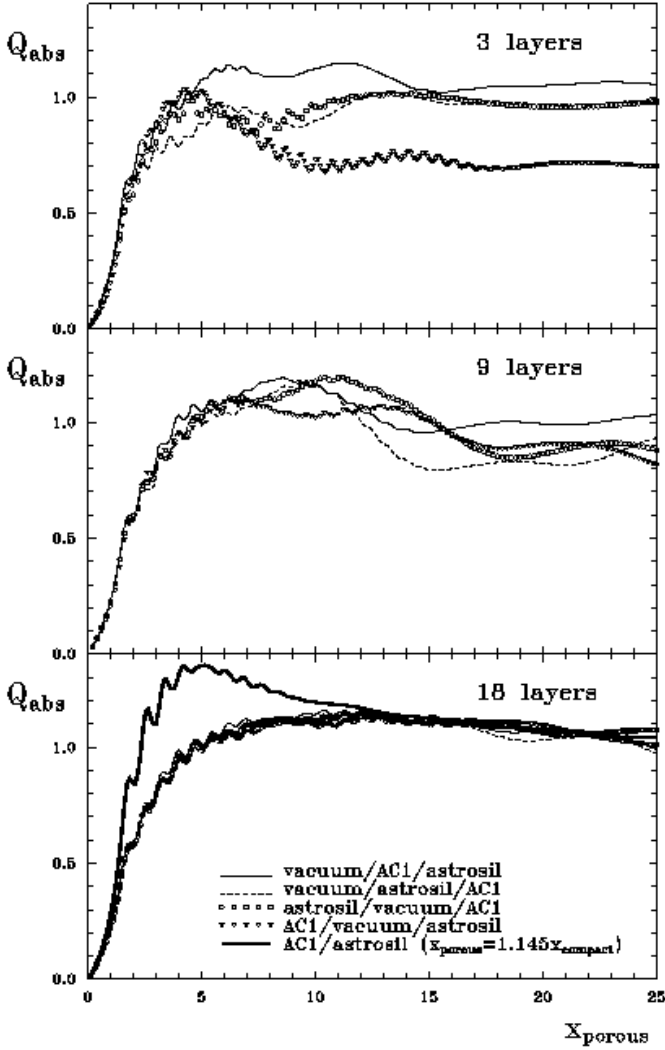


Fig. 4. The same as in Fig. 2 but now for absorption efficiency factors.

albedo Λ decreases when the porosity grows. Although the validity of these conclusions for particles beyond the Rayleigh domain remains unclear, the results of Hage & Greenberg (1990) are frequently used for estimates of grain properties in comets (see, e.g., Mason et al. 2001).

The role of porosity in dust optics was also analyzed by Krügel & Siebenmorgen (1994) who calculated the normalized absorption cross-sections

$$C^{(n)} = \frac{C(\text{porous grain})}{C(\text{compact grain of same mass})} = (1 - \mathcal{P})^{-2/3} \frac{Q(\text{porous grain})}{Q(\text{compact grain of same mass})}. \quad (3)$$

Effective optical constants of porous particles were calculated, in particular, using the Bruggeman mixing rule. The Mie theory was applied to get Q_{abs} . Krügel & Siebenmorgen found that the cross-sections $C_{\text{abs}}^{(n)}$ increased until $\mathcal{P} \lesssim 0.6$ and then decreased.

Figure 8 shows the extinction efficiencies and normalized cross-sections for multi-layered spheres of increasing

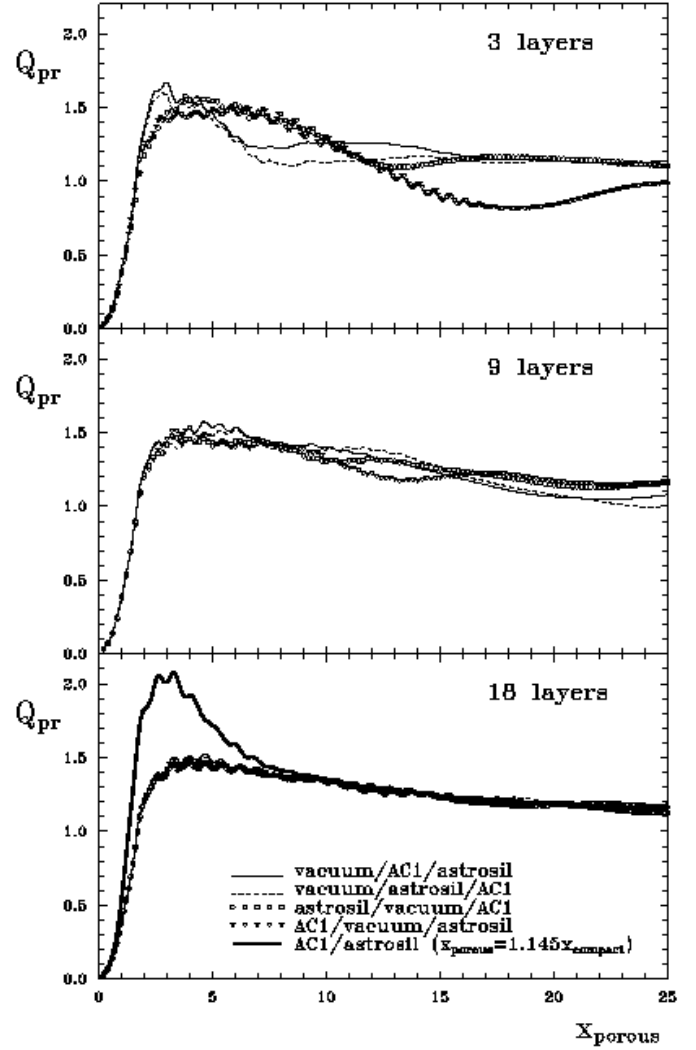


Fig. 5. The same as in Fig. 2 but now for radiation pressure efficiency factors.

porosity. The results are plotted in two scales: related to the real outer particle size parameter x and the size parameter calculated from the volume fraction of solid materials x_{compact} (Eq. (3)). It can be seen that the growth of porosity leads to the disappearance of the first maximum: the curves immediately approach the limiting value $Q_{\text{ext}} = 2$. It is important that the extinction factors generally decrease when \mathcal{P} increases¹ and the values of $C_{\text{ext}}^{(n)}$ almost always are greater than unity, i.e. porosity increases extinction. An opposite case is observed only in a restricted range of the size parameters $x_{\text{compact}} \approx 1 - 3$.

As follows from Fig. 9, such a behaviour of the extinction cross-sections is combined with the similar effects in scattering and absorption cross-sections. At the same time, the scattering efficiencies slightly grow and the absorption efficiencies significantly decrease for very porous

¹ A similar conclusion can be made from the DDA calculations of Wolff et al. (1994) who considered particles with \mathcal{P} up to 0.8.

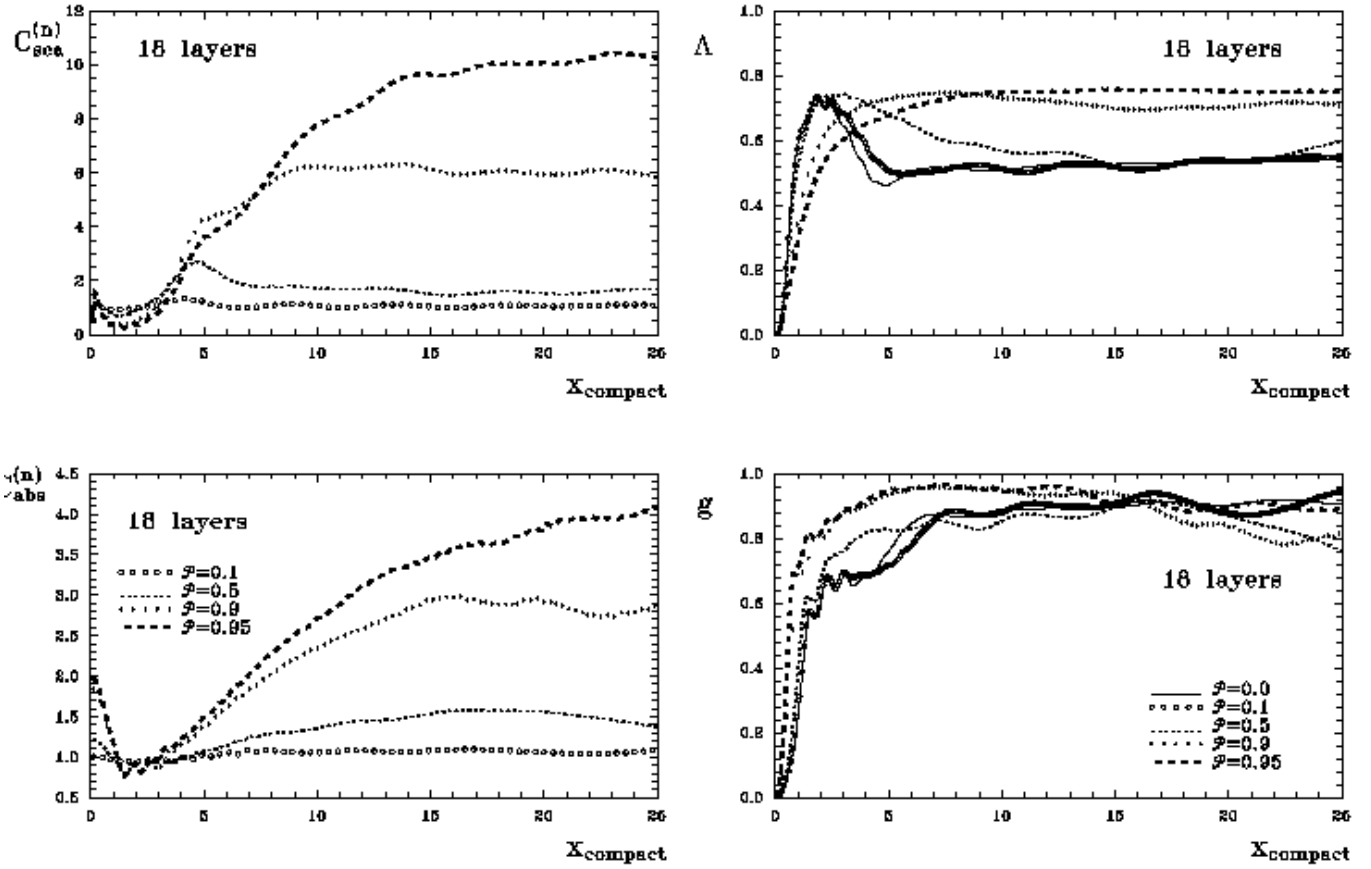


Fig. 9. Size dependence of the scattering and absorption normalized cross-sections, albedo and asymmetry parameter for multi-layered porous spheres. The parameters of particles are the same as in Fig. 8.

grains. Note also that both Λ (beginning with size parameter $x_{\text{compact}} \gtrsim 2 - 3$) and g (for particles of all sizes) increase with the particle porosity. The behaviour of $C_{\text{abs}}^{(n)}$ and Λ found by us is more complicated than predicted by Hage & Greenberg (1990). Namely, the growth of porosity leads to an increase of $C^{(n)}$ and an decrease of Λ for very small grains, and to an increase of both quantities for large grains. There exists also a small interval of particles of intermediate sizes where both $C^{(n)}$ and Λ decrease.

3. On the possibility to describe the optical properties of multi-layered particles with Effective Medium Theory

The EMT is an approach to treat inhomogeneous scatterers by homogeneous particles having an average (effective) refractive index. The EMT is well described in the recent reviews of Sihvola (1999), Chýlek et al. (2000) and papers of Spanier & Herman (2000) and Kolokolova & Gustafson (2001). There are many EMT rules, but besides a few ones they are rather similar in principle. Here we give formulas of the most often used EMT rules for n -component mixtures: the Garnett (1904) and Bruggeman (1935) rules. In the first case, the mixing rule averages the dielectric

permittivities of inclusion materials ε_i and a “matrix” (host) material ε_m ⁽²⁾

$$\varepsilon_{\text{eff}} = \varepsilon_m \left(1 + \frac{3 \sum_i f_i \frac{\varepsilon_i - \varepsilon_m}{\varepsilon_i + 2\varepsilon_m}}{1 - \sum_i f_i \frac{\varepsilon_i - \varepsilon_m}{\varepsilon_i + 2\varepsilon_m}} \right), \quad (4)$$

where $f_i = V_i/V_{\text{total}}$ is the volume fraction of the i th material and ε_{eff} is the effective permittivity. The expression for the Bruggeman (1935) rule is

$$\sum_i f_i \frac{\varepsilon_i - \varepsilon_{\text{eff}}}{\varepsilon_i + 2\varepsilon_{\text{eff}}} = 0. \quad (5)$$

As an example of a more sophisticated rule, we use the “layered-sphere EMT” introduced by VM. In this case, the effective optical constants ε_{eff} are defined as follows (see also Farafonov 2000):

$$\varepsilon_{\text{eff}} = \frac{1 + 2\alpha/V}{1 - \alpha/V} = \frac{\mathcal{A}_2}{\mathcal{A}_1}, \quad (6)$$

where α is the complex electric polarizability and the coefficients \mathcal{A}_1 and \mathcal{A}_2 are obtained as a result of multiplication of matrices depending on the optical constants of

² The dielectric permittivity is related to the refractive index as $\varepsilon = m^2$.

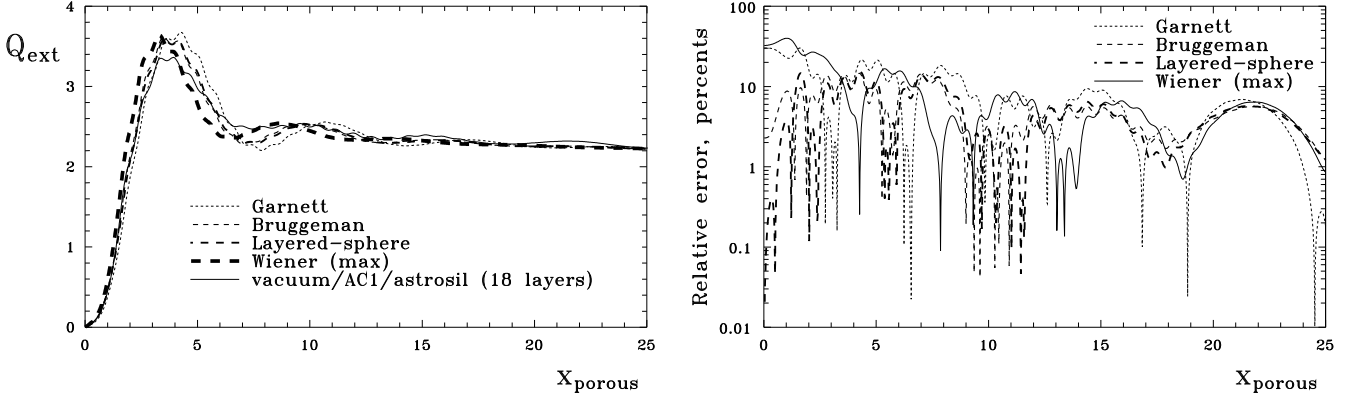


Fig. 10. Size dependence of the efficiency factors (left panel) and their relative errors (right panel) calculated with the exact theory for multi-layered spheres and with the Mie theory using four different EMT rules. Multi-layered particles contain an equal fraction of amorphous carbon (AC1), astrosil and vacuum. The cyclic order of the 18 layers is indicated.

layers and the volume fractions

$$\begin{aligned}
 \begin{pmatrix} \mathcal{A}_1 \\ \mathcal{A}_2 \end{pmatrix} &= \begin{pmatrix} 1 & 1/3 \\ \varepsilon_n & -2/(3\varepsilon_n) \end{pmatrix} \\
 &\times \prod_{i=2}^{n-1} \begin{pmatrix} 1/3 \left(\frac{\varepsilon_i}{\varepsilon_{i+1}} + 2 \right) & -2/(9f_i) \left(\frac{\varepsilon_i}{\varepsilon_{i+1}} - 1 \right) \\ -f_i \left(\frac{\varepsilon_i}{\varepsilon_{i+1}} - 1 \right) & 1/3 \left(2\frac{\varepsilon_i}{\varepsilon_{i+1}} + 1 \right) \end{pmatrix} \\
 &\times \begin{pmatrix} 1/3 \left(\frac{\varepsilon_1}{\varepsilon_2} + 2 \right) \\ -f_1 \left(\frac{\varepsilon_1}{\varepsilon_2} - 1 \right) \end{pmatrix}. \quad (7)
 \end{aligned}$$

The absolute bounds to ε_{eff} were given by Wiener (1910)

$$\varepsilon_{\text{eff, max}} = \sum_i f_i \varepsilon_i, \quad (8)$$

and

$$\varepsilon_{\text{eff, min}} = \left(\sum_i \frac{f_i}{\varepsilon_i} \right)^{-1}. \quad (9)$$

For any composition and structure, ε_{eff} has not to lie beyond these limits as long as the microstructural dimensions remain small compared with the radiation wavelength. Note that in the composite grain model of Mathis & Whiffen (1989) the effective refractive index was calculated from Eq. (8), i.e. the maximum of the permissible refractive indices was taken.

The general condition of EMT applicability is that the size of “inclusions” (in the EMT the particle inhomogeneity is considered in the form of uniformly distributed inclusions) is small in comparison with the wavelength of incident radiation (Chýlek et al. 2000). The real range of applicability of different rules was shown to be nearly the same (see, e.g., Table 4 in Voshchinnikov 2002).

Now let us discuss how different EMT rules can reproduce the optical properties of multi-layered spheres.

Figure 10 (left panel) shows the extinction efficiency factors computed with the exact theory for 18 layered spheres (the order of materials is vacuum/AC1/astrosil) and with the Mie theory using Garnett,³ Bruggeman, and layered-sphere mixing rules of the EMT. The effective refractive indices are equal to $m_{\text{eff}} = 1.496 + 0.060i$, $m_{\text{eff}} = 1.541 + 0.081i$ and $m_{\text{eff}} = 1.529 + 0.080i$ for Garnett, Bruggeman and layered-sphere mixing rules, respectively. Wiener’s maximum bound is $m_{\text{eff}} = 1.604 + 0.105i$. Figure 10 (right panel) demonstrates the relative errors for these EMTs. It can be seen that the errors of the Bruggeman and layered-sphere rules are of several percent or better in the considered range of particle sizes. The same is generally true for other efficiency factors and albedo. An exception is the region after the first maximum of the scattering efficiency factor and albedo ($x_{\text{porous}} \approx 6 - 8$) where the relative errors may reach up to 20%. The largest errors occur for the asymmetry factor, especially for small size parameters. The high accuracy of the layered-sphere rule in the case of very small particles sizes is explained by the fact that it is based on the Rayleigh approximation.

It should be noted that the order of materials playing a role, for particles with several layers (see Sect. 2.2), is also important for the considered 18-layered particles. For example, for spheres with another order of materials (e.g., AC1/vacuum/astrosil) the interference maxima are stronger than in the above-considered case (see Figs. 4, 5 and 8) and as a consequence, the relative errors for the EMT rules are larger, sometimes well exceeding 20%. Other rules of the EMT behave like the Garnett and Bruggeman rules, and we can conclude that despite the general condition of the EMT applicability is not fulfilled for layered particles – “inclusions” (layers) are not small in comparison with the wavelength of incident radiation – most rules of the EMT can reproduce the optical properties of layered spheres of any size, if the number of layers

³ Vacuum was adopted as a matrix.

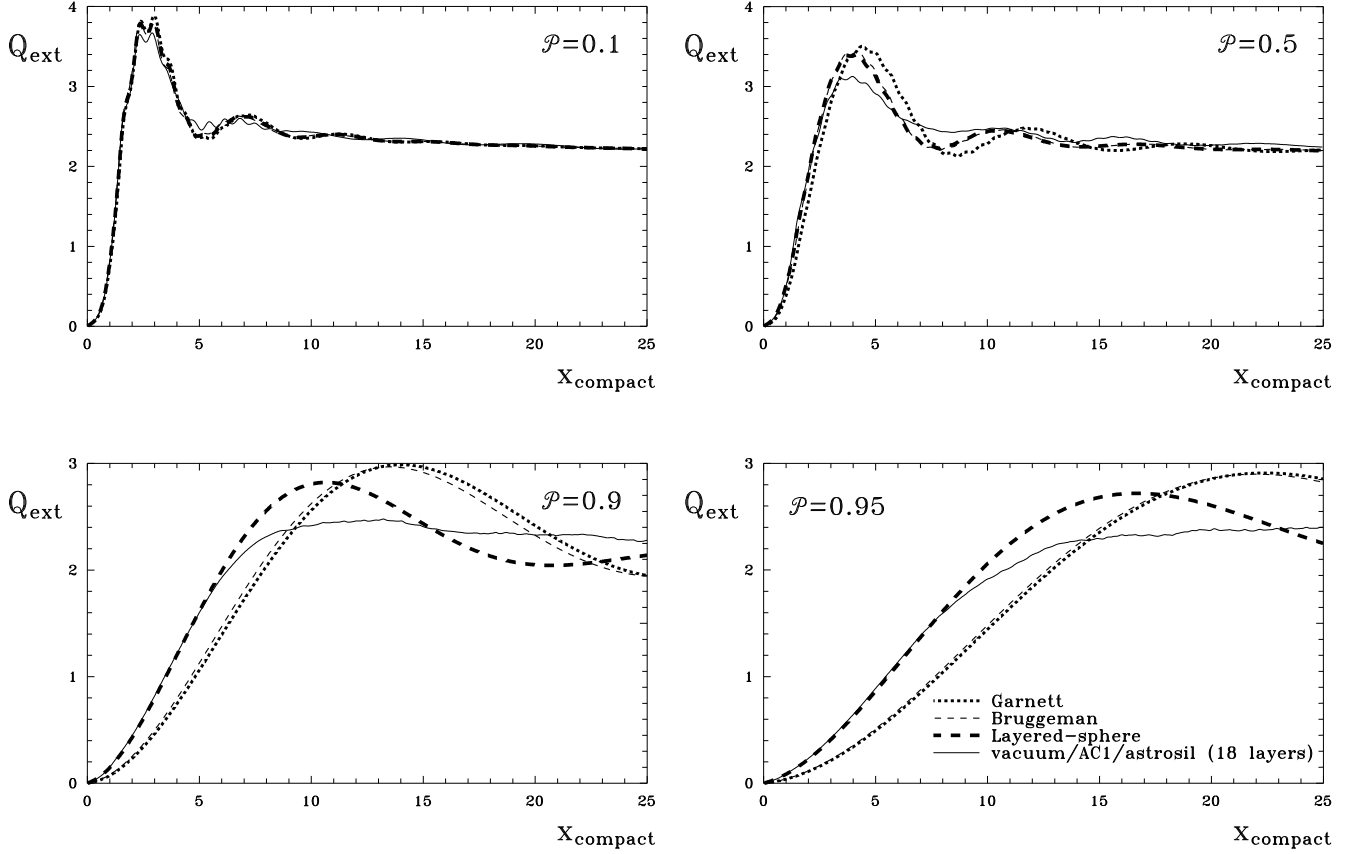


Fig. 11. Size dependence of the efficiency factors calculated with the exact theory for multi-layered spheres and with the Mie theory using three different EMT rules. Multi-layered particles consist of 18 layers (6 shells). Each shell contains the same volume fractions of AC1 and astrosil and a varied fraction of vacuum. The cyclic order of the layers is indicated.

is larger than 15 – 20. This conclusion can be, however, affected by the porosity of particles.

Figure 11 illustrates the applicability of different EMT rules to multi-layered spheres of varying porosity. The cases of other efficiency factors, albedo and asymmetry factor are similar. The Figure demonstrates that the layered-sphere rule has errors smaller than 10 – 20% for any porosity and size of particles, whereas other rules provide unacceptable approximations for large porosity ($\mathcal{P} \gtrsim 0.5$). From Fig. 11 (lower panels) one can see that the reason of this advantage of the layered-sphere rule is its accuracy in the Rayleigh domain ($x \rightarrow 0$). Here again other rules of the EMT behave like the Garnett and Bruggeman ones, and it can be concluded that if the multi-layered model provides a good approximation for particles with nearly homogeneous distribution of several materials, the classical EMT rules cannot be applied to strongly porous scatterers of this kind.

4. Wavelength dependence of extinction

As it is well known, the wavelength dependence of interstellar extinction $A(\lambda)$ is completely determined by

the wavelength dependence of the extinction efficiencies $Q_{\text{ext}}(\lambda)$. This quantity is shown in Fig. 12 for multi-layered particles of different sizes and porosity. The average interstellar extinction curve in the visible–near UV ($1 \mu\text{m}^{-1} \leq \lambda^{-1} \leq 3 \mu\text{m}^{-1}$) can be approximated by the power law $A(\lambda) \propto \lambda^{-1.33}$ (see discussion in Voshchinnikov 2002). This dependence is plotted in Fig. 12 as a dashed segment. From the Figure one can conclude that extinction depends on both the particle size and its chemical composition, i.e. the volume averaged refractive index. This mean refractive index is maximal for compact grains. Note that particles with 3 layers and those with 18 layers produce similar dependences $Q_{\text{ext}}(\lambda)$ in the visual part of the spectrum (Fig. 12, left panel).

As it has been mentioned many times (e.g., Greenberg 1978), a comparable extinction occurs if the product of the typical particle size $\langle r \rangle$ with the refractive index is constant

$$\langle r \rangle |m - 1| \approx \text{const.} \quad (10)$$

However, this conclusion breaks down if one considers very porous particles. The average refractive index of particles with larger fraction of vacuum shown in Fig. 12

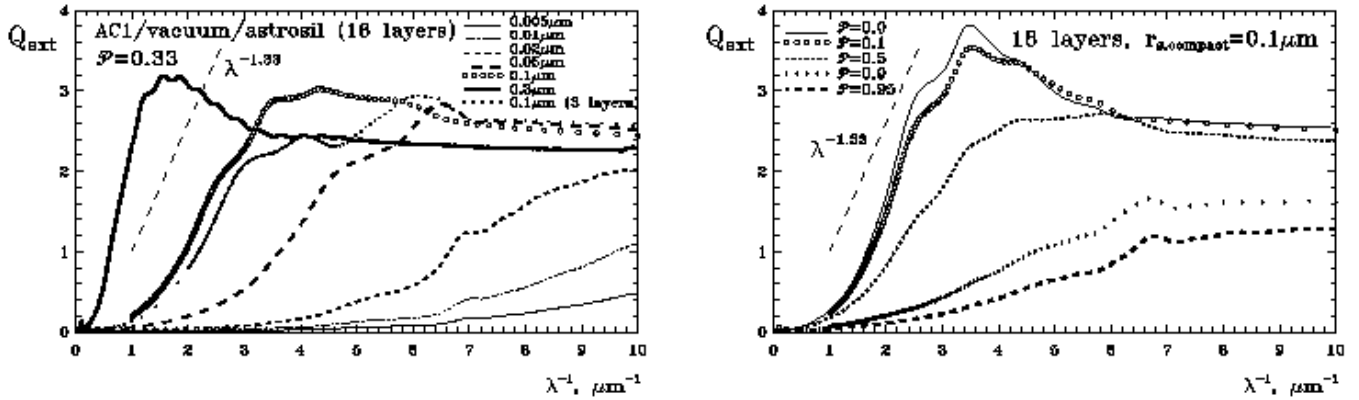


Fig. 12. Wavelength dependence of the extinction efficiency factors for multi-layered spherical particles. Left panel: particles of different sizes, each particle contains an equal fraction of AC1, astrosil and vacuum separated. The cyclic order of the layers is AC1/vacuum/astrosil. Right panel: particles of the same mass but of different porosity.

(right panel) is closer to 1 but their radii are larger (e.g., from Eq. (2) follows that $r_s = 0.27 \mu\text{m}$ if $\mathcal{P} = 0.95$ and $r_{s, \text{compact}} = 0.1 \mu\text{m}$). Despite of the equal amount of solid material in particles, the wavelength dependence of extinction becomes flatter. The analogous behaviour is typical of particles of other masses (i.e., for compact spheres of other radii), and, therefore, the reconstruction of the observed interstellar extinction curve with very porous grains only should will be rather difficult.

5. Radiation pressure

It is generally accepted that the mass loss in evolved stars is controlled by the radiation pressure on dust grains. The radiation pressure also affects the motion of interplanetary and interstellar grains. The capacity of a star with the effective temperature T_\star , radius R_\star and mass M_\star to move a grain with the radius r_s is characterized by the sweeping efficiency (the ratio of the radiation pressure force to the gravitational one, see, e.g., Voshchinnikov & Il'in 1983)

$$\beta \equiv \frac{F_{\text{pr}}}{F_g} = \frac{\sigma}{cG} \frac{R_\star^2 T_\star^4}{M_\star} \frac{\pi r_s^2 \bar{Q}_{\text{pr}}}{\rho_d V}. \quad (11)$$

Here, σ is the Stephan-Boltzmann constant, c the speed of light, G the gravitational constant, V the particle volume, ρ_d the material density, \bar{Q}_{pr} the Planck mean radiation pressure efficiency.

Figure 13 shows the size dependence of β for multi-layered porous and compact spheres. The radius of porous particles is calculated from Eq. (2) and their density is given in Table 1. As follows from Fig. 13, an increase of particle porosity results in the increase of the sweeping efficiency for small particles ($r_{s, \text{compact}} \lesssim 0.1 \mu\text{m}$) and the decrease of β for large particles ($r_{s, \text{compact}} \gtrsim 0.1 \mu\text{m}$). For very porous grains, the dependence $\beta(r_s)$ is flat, i.e. almost size independent. So, the motion of such particles will be determined by the drag force due to collisions with gas particles.

Previous calculations of radiation pressure on porous particles have been made, using Mie theory and the Bruggeman mixing rule (Il'in & Krivova 2000) and the DDA for fluffy dust aggregates (Kozasa et al. 1992, Kimura et al. 2002). The behaviour of the sweeping efficiency for aggregates of increasing porosity (the DDA calculations) seems to be similar to that found by us while the Mie–Bruggeman theory leads to the results contradicting those presented in Fig. 13.

6. Scattered radiation

6.1. Albedo and asymmetry parameter

In modelling of light scattering in dusty objects, the Henyey & Greenstein (1941) phase function is often used. It is parameterized by the asymmetry parameter g . Then albedo Λ and g are utilized as parameters for radiative transfer problems irrelevant to the actual properties of dust grains.

The standard behaviour of albedo and asymmetry parameter is as follows: $\Lambda \ll 1$ and $g \simeq 0$ for small size parameters (small sizes or large wavelengths), then Λ and g grow with increasing particle size or decreasing wavelength and reach the asymptotic values for very large size parameters. The behaviour of Λ vs. g is plotted in Fig. 14 for porous and compact particles. It is important to keep in mind that the albedo and asymmetry parameter cannot be determined from observations separately, but only together (as a combination). Therefore, models with one fixed parameter and the other varying often make little physical sense. We only mention the paper of Witt & Gordon (2000) who compiled the results of the determination of Λ and g for galactic dust from 13 publications. These data are mainly based on the previous modelling of scattered light from reflection nebulae and diffuse galactic light in the visual and UV parts of spectrum. Witt & Gordon visually averaged the wavelength dependencies of albedo and asymmetry parameter and shifted the data

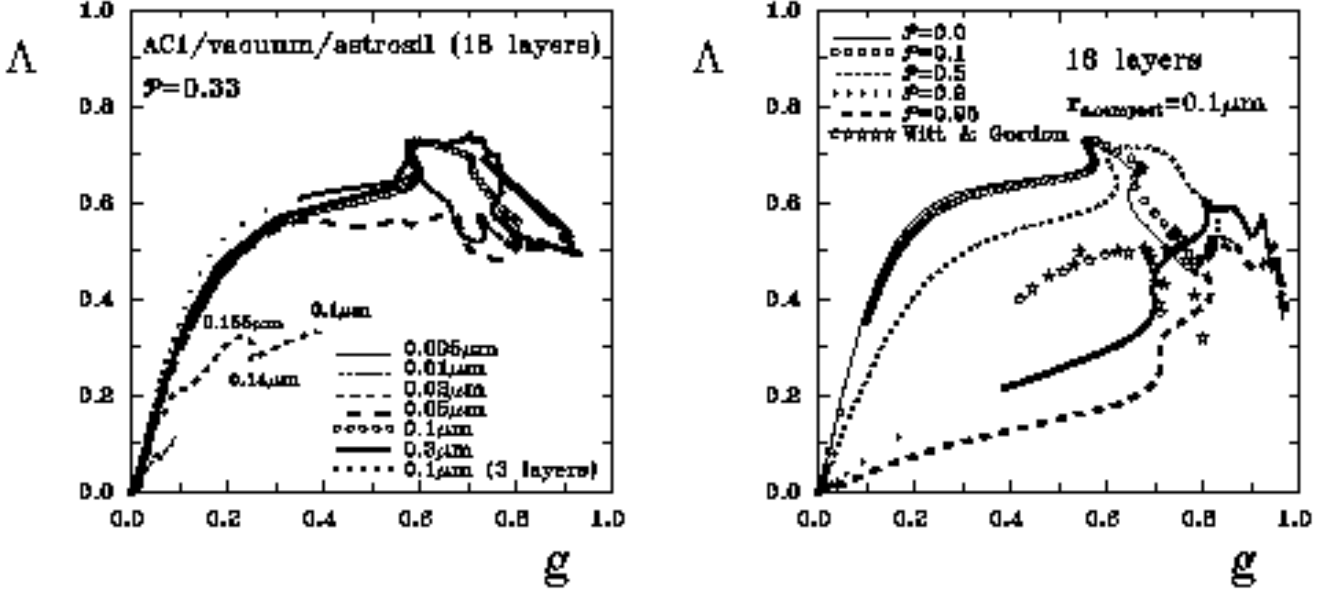


Fig. 14. Albedo dependence on the asymmetry parameter for multi-layered spherical particles. The particle parameters are the same as in Fig. 12. All curves start at the wavelength $\lambda = 20 \mu\text{m}$, where $\Lambda \simeq g \simeq 0$, and finish at $\lambda = 0.1 \mu\text{m}$. The turning points for the particle with $r_{s, \text{compact}} = 0.02 \mu\text{m}$ are marked at the left panel. At the right panel, the stars present the summary results of determination of Λ and g in the wavelength range $\lambda = 0.1 - 3.0 \mu\text{m}$ for our Galaxy (Witt & Gordon, 2000, Table 1; see also discussion in the text).

for Λ to reach agreement with the dust model of Kim et al. (1994). As a result, the dependencies $\Lambda(\lambda)$ and $g(\lambda)$ for wavelengths $\lambda = 0.1 - 3.0 \mu\text{m}$ were published in tabular and graphical forms. These data are shown in Fig. 14 (right panel). It can be seen that depending on the particle size and wavelength of radiation the position of any particle in the $\Lambda - g$ plane is well fixed. *Some pairs of parameters (Λ , g) have no correspondence to any particle.* In particular, in order to fill in the right lower corner in such diagrams, the particles should be very porous ($\mathcal{P} \gtrsim 0.7$). Note that neither Witt & Gordon (2000), nor Kim et al. (1994) considered porous grains. The theoretical constraints on the albedo and asymmetry parameter were also discussed by Chlewicki & Greenberg (1984) who showed that the results of some models could not be realized by the optics of small particles.

6.2. Intensity and polarization

The angular dependence of the intensity of scattered radiation is mainly determined by the particle size parameter (van de Hulst 1957, Bohren & Huffman 1983). This is well seen when the normalized intensity is considered. Variations in the order of layers have a small effect on the intensity in the case of scattering in the forward hemisphere (the scattering angles $\Theta < 90^\circ$, Fig. 15, left upper panel). In the backward hemisphere ($\Theta > 90^\circ$), the dependencies of $I(\Theta)$ for particles consisting of 18 layers being compact or having intermediate porosity ($\mathcal{P} = 0.33$) are

similar. Note that the order of layers becomes important for three-layered particles at $\Theta \gtrsim 120^\circ$.

The influence of the particle porosity on the normalized intensity is shown in Fig. 15 (right upper panel). The growth of porosity is accompanied by an increase of the particle size because the particle mass is fixed. In the case of very large values of \mathcal{P} , the intensity strongly grows for nearly forward directions ($\Theta \lesssim 40^\circ$), which looks similar to the behaviour of intensity for large transparent spheres.

In contrast to the intensity, the polarization of the scattered radiation strongly depends on the order of layers in the particle as well as its porosity (see Fig. 15, lower panels). Very large differences in polarization occur at almost all scattering angles. The change of the order of layers and the porosity can result in a change of the sign of polarization. In the case of the three-layered particles (Fig. 15, left lower panel), the polarization is mainly positive if vacuum is in the core and the polarization is mainly negative if vacuum forms an intermediate layer. At large scattering angles ($\Theta \gtrsim 110^\circ$), the negative polarization transforms to the positive one when \mathcal{P} increases (Fig. 15, right lower panel).

7. Infrared radiation

7.1. Temperature

The commonly considered equilibrium temperature of cosmic grains is the result of absorption of the UV and visual

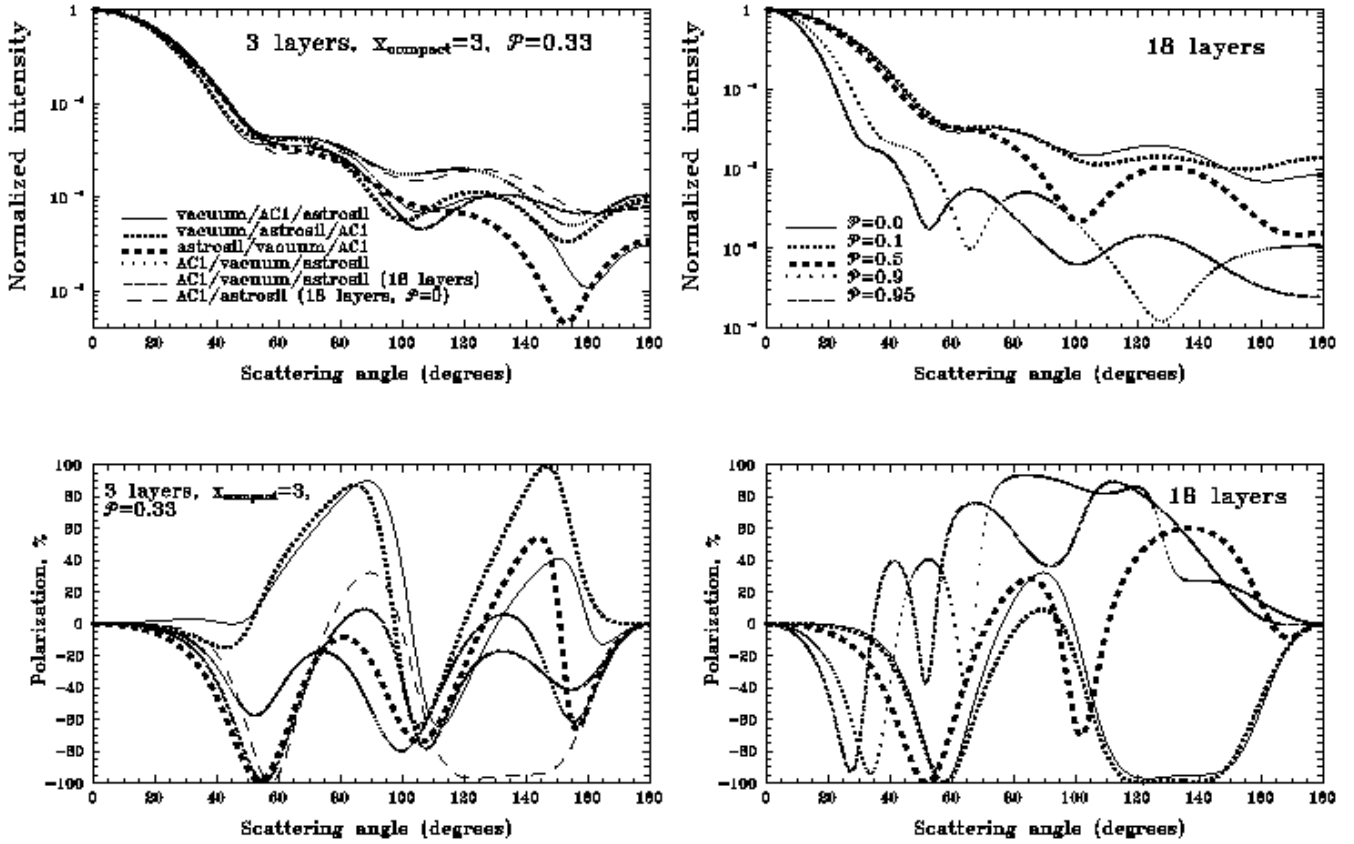


Fig. 15. Normalized intensity and polarization of scattered radiation for multi-layered spheres. Left panels: particles of the same size ($x_{\text{compact}} = 3$) but different cyclic order of the layers. Right panels: particles of the same mass but different porosity. the cyclic order of the layers is AC1/vacuum/astrosil.

stellar photons and re-emission of IR photons. Figure 16 shows the temperature of multi-layered particles, depending on their size. The results were calculated for particles located at a distance of $10^4 R_\star$ from a star with the effective temperature $T_\star = 2500$ K. In all cases, the increase of the vacuum volume fraction causes a decrease of the grain temperature if the amount of the solid material is kept constant. This result holds for particles of larger sizes located closer to (or farther from) the star and for other values of T_\star . If the materials are well mixed (the number of shells $\gtrsim 3 - 4$), the temperature drops when the porosity grows. Such a behaviour contradicts the results of Greenberg & Hage (1991) who found an increase of temperature with grain porosity (see their Fig. 4). The discrepancy is explained by the impossibility of the method used by Greenberg & Hage to treat very porous particles (see also Sect. 7.2).

If the materials are badly mixed, the grain temperature is determined by the position of the most absorbing component (amorphous carbon) in the particle. If AC1 is in the core (“stars” in Fig. 16), the temperature will be 3 – 6 K lower than in the case when AC1 forms an intermediate or outermost layer.

7.2. Infrared features

As it is well known, the shape of IR dusty features is a good indicator of particle size and chemical composition. With increasing size, a feature becomes wider and wider and fades away. For example, in the case of compact spherical grains of astrosil, the $10 \mu\text{m}$ and $18 \mu\text{m}$ features disappear when the grain radius exceeds $\sim 2 - 3 \mu\text{m}$. The small scale structure of features are usually attributed to the variations of components of grain material (e.g., changes of the ratio of magnesium to iron in silicates) or the modification of the material state (amorphous/crystalline).

In Fig. 17 we compare the wavelength dependence of the absorption efficiency factors for particles of the same mass but different structure. The upper panel shows the results for particles of the same porosity consisting of one shell (three layers). In this case, the central position and the width of dust features depend on the order of layers. Larger changes occur for the red wing. Note that the normalized factors are very similar for particles of different sizes (if $r_{\text{s, compact}} \lesssim 0.5 \mu\text{m}$) and vary only with particle structure. As in the previous cases, with the increase of the number of layers the results converge to some limit (thick solid curve in Fig. 17).

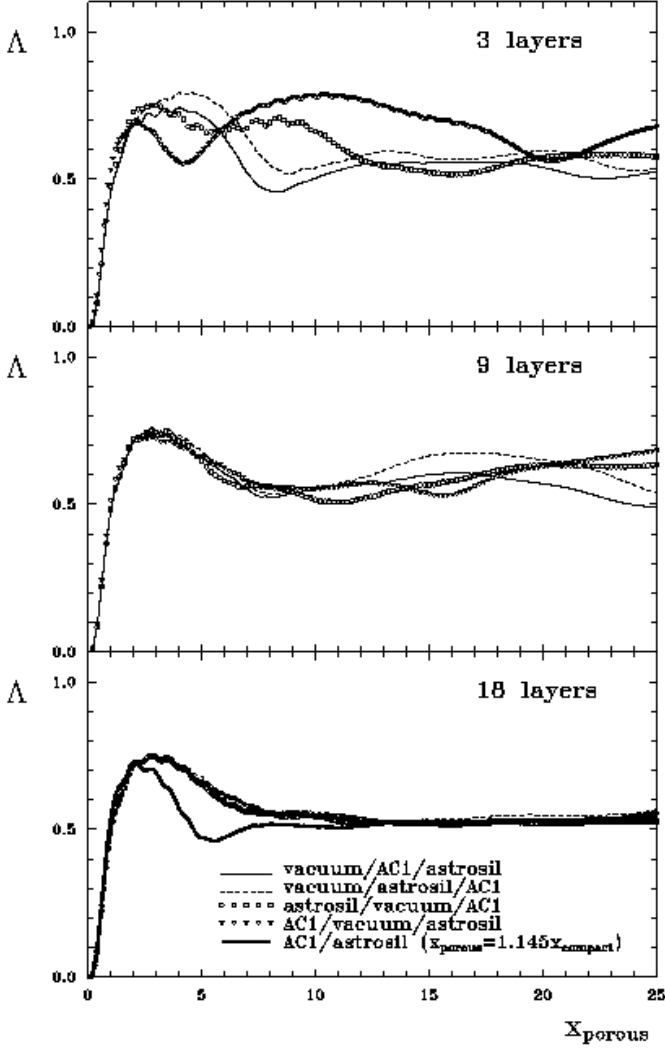


Fig. 6. The same as in Fig. 2 but now for albedo.

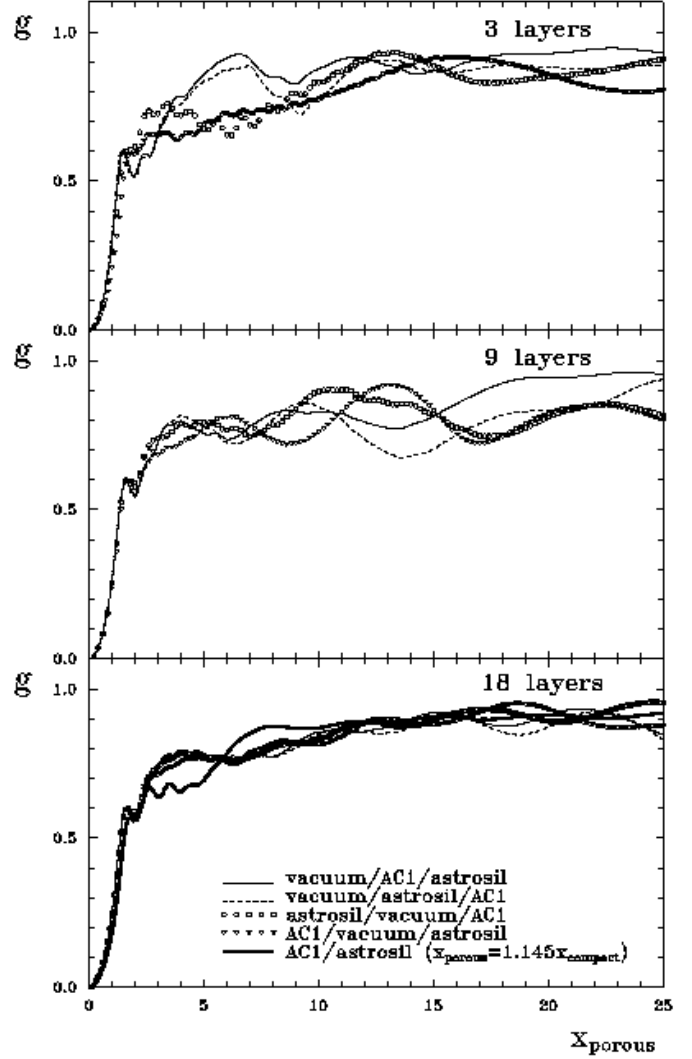


Fig. 7. The same as in Fig. 2 but now for asymmetry parameter.

In the lower part of Fig. 17, variations of Q_{abs} with the particle porosity are plotted. The growth of \mathcal{P} causes of the shift the center of the feature to longer wavelengths and its broadening. For particles with $\mathcal{P} = 0.95$, the $10 \mu\text{m}$ feature transforms into a plateau while the $18 \mu\text{m}$ feature disappears. This tendency is opposite to the results shown in Fig. 7 of Hage & Greenberg (1990) who found that the higher the porosity, the sharper the silicate emission becomes, but agrees with the DDA calculations of Henning & Stognienko (1993).

Their model was used later by Li & Greenberg (1998) for the explanation of the $10 \mu\text{m}$ emission feature in the disc of β Pictoris. The best fitting was obtained for highly porous particles with $\mathcal{P} \approx 0.95$. In order to estimate the validity of this conclusion, we plotted in Fig. 18 our data from Fig. 17 in a normalized manner together with observations of β Pictoris made by Knacke et al. (1993) and Telesco & Knacke (1991). As follows from Fig. 18, the observed shape of the silicate feature is better reproduced if particles are compact or the porosity is small.

7.3. Dust opacities

The dust opacity or the mass absorption coefficient of a grain material $\kappa(\lambda)$ enters directly in the expression for the dust mass of an object M_d which is determined from IR observations

$$M_d = \frac{F_{\text{IR}}(\lambda) D^2}{\kappa(\lambda) B_\lambda(T_d)}. \quad (12)$$

Here, $F_{\text{IR}}(\lambda)$ is the observed flux, D the distance to the object, $B_\lambda(T_d)$ the Planck function, T_d the dust temperature. The quantity $\kappa(\lambda)$ depends on the particle volume V , the material density ρ_d and the extinction cross-section C_{ext}

$$\kappa(\lambda) = \frac{C_{\text{ext}}}{\rho_d V} \approx \frac{3}{\rho_d} \left(\frac{2\pi}{\lambda} \right) \text{Im} \left\{ \frac{\alpha}{V} \right\} = \frac{3}{\rho_d} \left(\frac{2\pi}{\lambda} \right) \text{Im} \left\{ \frac{\varepsilon_{\text{eff}} - 1}{\varepsilon_{\text{eff}} + 2} \right\}. \quad (13)$$

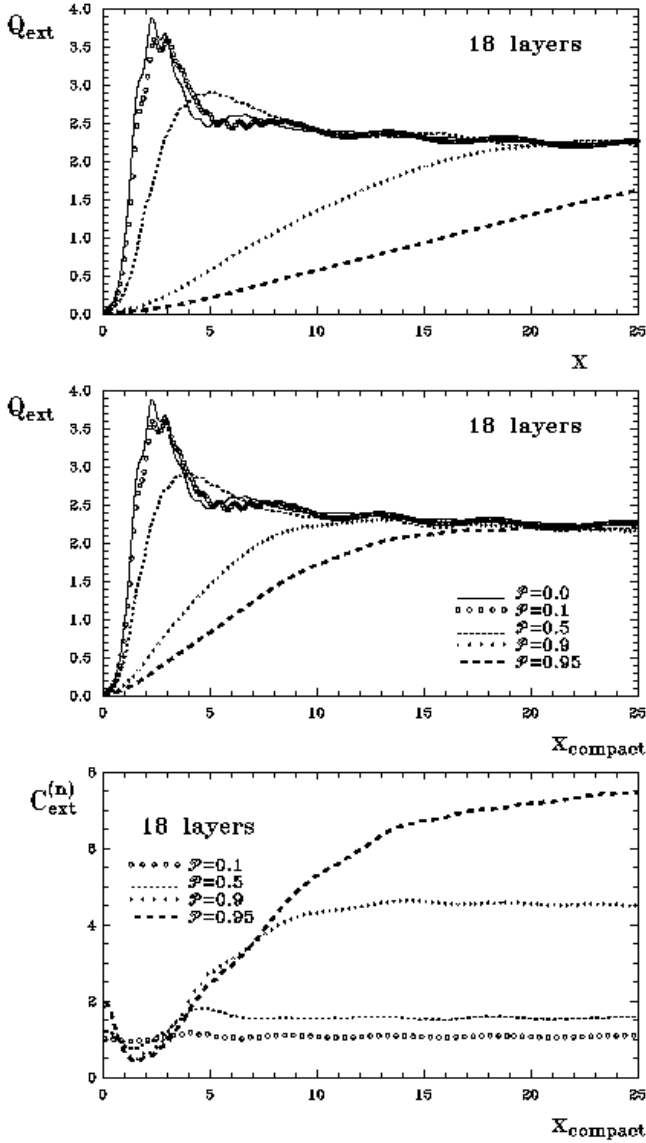


Fig. 8. Size dependence of the extinction efficiency factors for multi-layered spherical particles. Each particle consists of 18 layers (6 shells). Each shell contains the same volume fractions of AC1 and astrosil and a varied fraction of vacuum. The cyclic order of the layers is AC1/vacuum/astrosil. The effect of the increase of the particle porosity is illustrated. The factors Q_{ext} are plotted in dependence on the size parameter corresponding the outer particle radius (upper panel) and the size parameter corresponding to the volume fraction of solid materials (see Eq. (2); middle panel). The lower panel shows the normalized extinction cross-sections calculated according to Eq. (3).

At long wavelengths the scattering can be neglected and $C_{\text{ext}} \approx C_{\text{abs}}$. We also can evaluate C_{abs} in the Rayleigh approximation, then the mass absorption coefficient will not depend on the particle size as follows from the right part of Eq. (13). The effective dielectric permittivity in

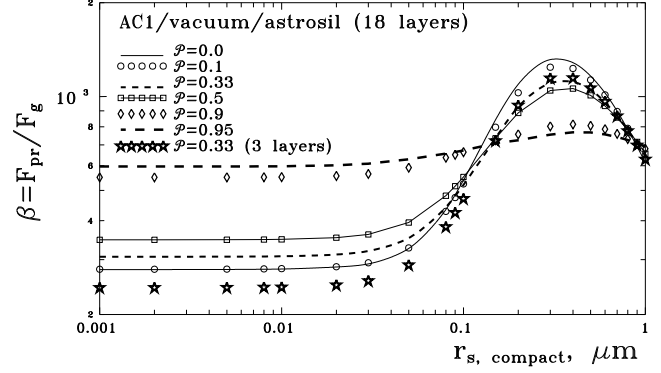


Fig. 13. Size dependence of the sweeping efficiency for multi-layered spheres. The cyclic order of the layers is AC1/vacuum/astrosil. The particles are located near a star with the effective temperature $T_{\star} = 2500$ K, radius $R_{\star} = 300 R_{\odot}$ and mass $M_{\star} = 2 M_{\odot}$.

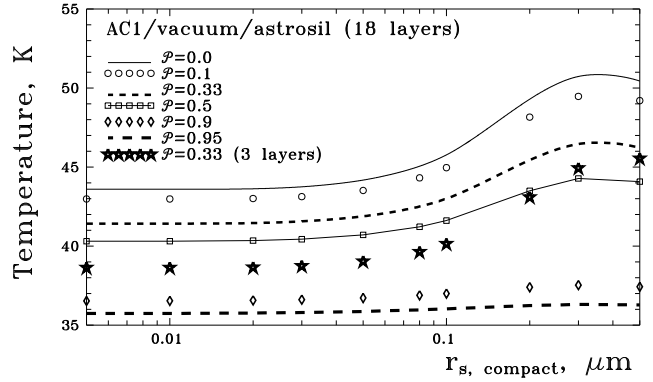


Fig. 16. Size dependence of the temperature for multi-layered spheres. The cyclic order of the layers is AC1/vacuum/astrosil. The particles are located at a distance of $10^4 R_{\star}$ from a star with the effective temperature $T_{\star} = 2500$ K. The radius of porous particles is calculated from Eq. (2).

Eq. (13) can be found from the layered-sphere rule of the EMT (see Eqs. (6), (7)).

Extensive study of the dependencies of the mass absorption coefficients on the material properties and grain shape is summarized in the paper of Henning (1996) where, in particular, it is noted that the opacities at 1 mm are considerably larger for non-spherical particles in comparison with spheres (see also Ossenkopf & Henning 1994). We find that the similar effect yields the inclusion of vacuum as a component of composite particles. This follows from Table 1 where the opacities at $\lambda = 1$ mm are given for spheres of the same mass. It can be seen that the values of κ are generally larger for particles with larger fraction of vacuum and in the case of amorphous carbon as an outer layer. The last effect is reduced when the number of layers increases. Note that the growth of the opacity with

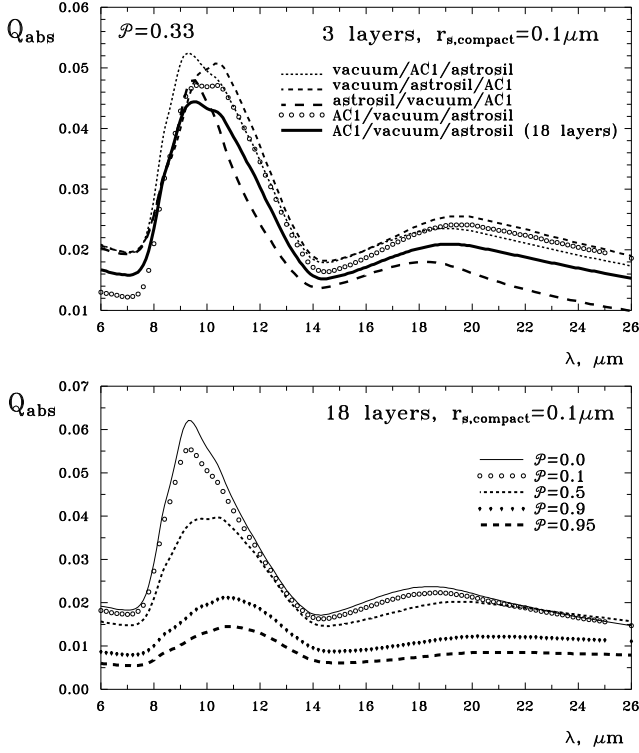


Fig. 17. Wavelength dependence of the absorption efficiency factors for multi-layered spherical particles.

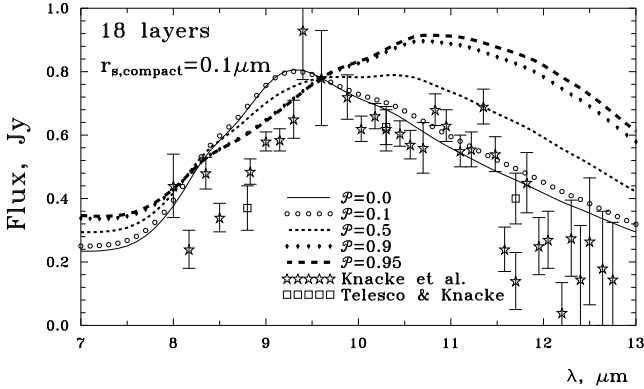


Fig. 18. Emission in the disc around the star β Pictoris in the region of silicate $10\,\mu\text{m}$ band. Stars and squares are the observations of Knacke et al. (1993) and of Telesco & Knacke (1991). The curves present the results of calculations for multi-layered particles of radius $r_{s,\text{compact}} = 0.1\,\mu\text{m}$ as shown in Fig. 17 but normalized at $\lambda = 9.6\,\mu\text{m}$.

particle porosity is related to the decrease of the particle density ρ_d which is calculated as the volume-average quantity. Because the mass of dust in an object is proportional to ρ_d (see Eqs. (12) and (13)), the assumption on porous grains leads to smaller masses.

Table 1. Opacities at $\lambda = 1\,\text{mm}$ of multi-layered and compact spheres of the same mass.

Particle	\mathcal{P}	$\rho_d, \text{g/cm}^3$	$\kappa, \text{cm}^2/\text{g}$
18 layers: AC1*/astrosil**	0.00	2.58	0.948
3 layers: vac/AC1/astrosil	0.33	1.72	2.84
vac/astrosil/AC1	0.33	1.72	3.63
astrosil/vac/AC1	0.33	1.72	3.41
AC1/vac/astrosil	0.33	1.72	1.37
18 layers: vac/AC1/astrosil	0.33	1.72	2.25
vac/astrosil/AC1	0.33	1.72	2.22
astrosil/vac/AC1	0.33	1.72	2.39
AC1/vac/astrosil	0.33	1.72	1.96
18 layers: AC1/vac/astrosil	0.10	2.32	1.55
	0.30	1.73	2.20
	0.50	1.29	2.57
	0.70	0.772	4.04
	0.90	0.258	8.12
	0.95	0.129	10.4

* $m(1\text{mm}) = 2.93 + 0.276i$, $\rho_d = 1.85\,\text{g/cm}^3$

** $m(1\text{mm}) = 3.43 + 0.050i$, $\rho_d = 3.3\,\text{g/cm}^3$

8. Multi-layered grains and cosmic abundances

8.1. Interstellar abundances and extinction

The basic requirement for any model of interstellar dust is the explanation of the observed extinction law taking into account the dust-phase abundances of elements in the interstellar medium. These abundances are obtained as the difference between the observed gas-phase abundances and the cosmic reference ones. However, the cosmic abundances are not yet conclusively established and usually this causes a problem. For many years, the solar abundances were used as the reference ones, until the photospheres of the early-type stars were found not to be so rich in heavy elements as the Sun was (Snow & Witt 1996). Such a revision of the reference abundances caused the so-called “carbon crisis”: abundances of the most important dust-forming elements (C, O, Mg, Si, Fe) required by the current dust models are greater than the abundances available in the solid phase of the interstellar medium. In the modelling of the interstellar extinction the solar abundances are still utilized (e.g., Weingartner & Draine 2001, Clayton et al. 2003), although high-resolution X-ray spectroscopy has already given direct evidence of the sub-solar interstellar abundance of oxygen. Using the Chandra high resolution spectrum of the object Cyg X-2, Takei et al. (2002) estimated the dust-phase ($179\,\text{ppm}^4$) and total ($579\,\text{ppm}$) abundances of oxygen. The latter is $\sim 68\%$ of the solar one ($851\,\text{ppm}$).

Our model of multi-layered porous particles is applied for the explanation of the absolute extinction in the direc-

⁴ particles per million hydrogen atoms

tion to two stars. The model could provide more extinction per unit of mass than models with compact particles (see Fig. 8, lower panel). There were many unsuccessful attempts to resolve the crisis. Here we analyse the principal possibility to do that and to enlarge the extinction per unit of mass in order to minimize the amount of solid phase substance. We considered several materials as components of composite grains. Among the carbonaceous species, the amorphous carbon in the form of BeI (Rouleau & Martin 1991) was found to produce the largest extinction. Also the extinction of iron oxides strongly increases with the growth of porosity.

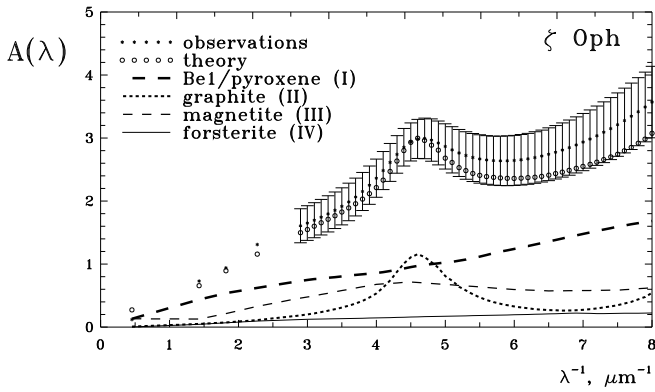


Fig. 19. Observed and calculated extinction in the direction to the star ζ Oph. The errors of the observations are the result of a parameterization of the observations (see Fitzpatrick & Massa 1990). The contribution to the theoretical extinction from different components is shown.

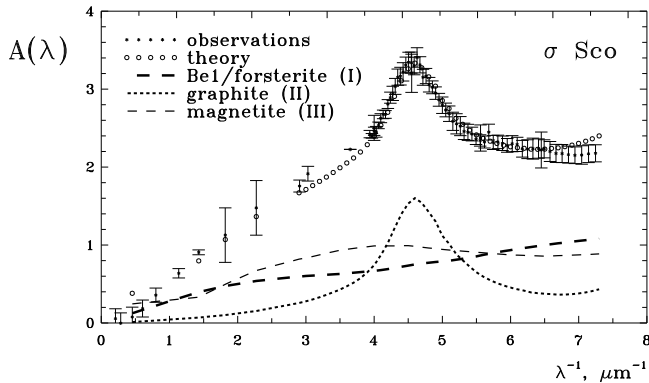


Fig. 20. The same as in Fig. 19 but now for the star σ Sco. The observational data were taken from Wegner (2002).

We fitted the observed extinction toward the stars ζ Oph (Fig. 19) and σ Sco (Fig. 20). The models consist of three or four grain populations.

- (I). Porous composite (multi-layered) particles (BeI — 5%, pyroxene, $\text{Fe}_{0.5}\text{Mg}_{0.5}\text{SiO}_3$ — 5% for ζ Oph or

forsterite, Mg_2SiO_4 — 5% for σ Sco and vacuum — 90%) with the power-law size distribution having an exponential decay. The lower/upper cut-off in the size distribution is $0.005\text{ }\mu\text{m}/0.25\text{ }\mu\text{m}$ and $0.05\text{ }\mu\text{m}/0.35\text{ }\mu\text{m}$ in the case of ζ Oph and σ Sco, respectively.

- (II). Small compact graphite grains with the narrow power-law size distribution ($r_s \approx 0.01 - 0.02\text{ }\mu\text{m}$).
- (III). Porous composite grains of magnetite (Fe_3O_4 — 2%, vacuum — 98%) with the power-law size distribution. The lower/upper cut-off in the size distribution is $0.005\text{ }\mu\text{m}/0.25\text{ }\mu\text{m}$ and $0.09\text{ }\mu\text{m}/0.50\text{ }\mu\text{m}$ in the case of ζ Oph and σ Sco, respectively.
- (IV). Compact grains of forsterite (Mg_2SiO_4) with the power-law size distribution (only for ζ Oph, $r_{s,\text{min}} = 0.005\text{ }\mu\text{m}$, $r_{s,\text{max}} = 0.25\text{ }\mu\text{m}$).

The contributions from different components to the calculated extinction are shown in Figs. 19 and 20.

Table 2. Interstellar “cosmic” and dust-phase abundances (in ppm)

Element	“cosmic” abundance	ζ Oph obs	ζ Oph model	σ Sco obs	σ Sco model
C	214	79	195	145	121
O	457	126	128	85	66
Mg*	25	23	25	22	15.5
Si	18.6	17	30	16.8	7.5
Fe	27	27	34	26.7	26.4

* The abundance of Mg was recalculated with the new oscillator strengths from Fitzpatrick (1997).

Table 2 gives the reference “cosmic” abundances of five dust-forming elements according to Snow & Witt (1996) as well as the observed and model dust abundances.

The dust-phase abundances in the line of sight to the star ζ Oph (HD 149757) were taken from Table 2 of Snow & Witt (1996). In our calculations, we adopted for ζ Oph: the total extinction $A_V = 0^{\text{m}}.94^{(5)}$, colour excess $E(B - V) = 0^{\text{m}}.32$ and the total hydrogen column density $N(\text{H}) = 1.35 \cdot 10^{21}\text{ cm}^{-2}$ (Savage & Sembach, 1996). The extinction curve was reproduced according to the parameterization of Fitzpatrick & Massa (1990).

For σ Sco (HD 147165), we used the extinction curve, colour excess $E(B - V) = 0^{\text{m}}.35$ and the total extinction $A_V = 1^{\text{m}}.13$ according to Wegner (2002). The hydrogen column density $N(\text{H}) = 2.46 \cdot 10^{21}\text{ cm}^{-2}$ was adopted from Zubko et al. (1996). The gas-phase abundances were taken from Allen et al. (1990).

The dust-phase abundances required by the model are larger than the observed ones in the direction to ζ Oph and smaller than the observed abundances in the direction to σ Sco. Note that for this star the required amount of C and

⁵ This value was obtained from the relation $A_V = 1.12 E(V - K)$ (Voshchinnikov & Il’in 1987) and colour excess $E(V - K) = 0^{\text{m}}.84$ (Serkowski et al. 1975).

Si in dust grains is the lowest in comparison with previous modelling. This is a result of the use of highly porous particles which gives the considerable extinction and simultaneously allows one to “save” the material. For example, the extinction model of σ Sco with compact grains presented by Zubko et al. (1996) requires 240 – 260 ppm of C and 20 – 30 ppm of Si and the model of Clayton et al. (2003) needs 155 ppm of C and 36 ppm of Si (cf. 121 ppm and 7.5 ppm from Table 2).

Evidently, it remains an open question how to explain the observed values of extinction of different stars with a reduced amount of heavy elements (i.e. how to increase the extinction to volume ratio). It seems that some enhancement of this ratio can be expected if one takes into account a possible non-sphericity of dust grains, but it is difficult to believe that this improvement will completely resolve the problem (see Fig. 29 in Voshchinnikov 2002). It is also hardly probable that larger extinction values are provided by an unknown material. The possible way to overcome the carbon crisis may be a re-examination of the reference cosmic abundances and a detailed study of their local dependencies.

8.2. Iron as a component of multi-layered particles

Iron being highly depleted in the interstellar medium is one of the major dust-forming elements (Snow & Witt 1996, Jones 2000). According to the recent results of Snow et al. (2002) obtained with the Far Ultraviolet Spectroscopic Explorer (FUSE), the abundance of iron in the dust-phase is in the range from 95.2% to 99.6% of the cosmic abundance. Iron can be incorporated into dust grains in the form of oxides (FeO , Fe_2O_3 , Fe_3O_4), (Mg, Fe)-silicates, sulfides and metallic iron. The last possibility causes from the theory of dust condensation in circumstellar environments (Lewis & Ney 1979, Gail & Sedlmayr 1999). Gail & Sedlmayr (1999) note that iron starts to condense at a temperature well below the stability limits of some silicates like forsterite and quartz. This leads to condensation of iron on the surface of silicate grains where iron islands can be formed. The continuing growth of the islands will be accompanied by condensation of new silicate layers and, finally, a layered particle arise. The fraction of iron incorporated into grains in the form of metallic Fe is inversely proportional to the stellar mass-loss rate (Ferratori & Gail 2001).

Metallic iron was considered several times as a separate component of dust mixtures in the modelling of spectral energy distribution of OH/IR stars (Harwit et al. 2001, Kemper et al. 2002), Herbig Ae/Be stars (Bouwman et al. 2000), protostellar objects (Demyk et al. 1999). The main reason of the inclusion of iron is its great opacity in the near-infrared spectral range. Usually the required mass fraction of metallic iron is several percent (Bouwman et al. 2000, Kemper et al. 2002). However, sometimes iron is assumed to be the main component of the dust mixture (Harwit et al. 2001). In order to increase the opacity of

iron particles further and correspondingly to decrease the mass fraction of iron the shape of grains was considered to be needle-like (Kemper et al. 2002) that strongly increases the radiation pressure on them and cuts down their lifetime in stellar atmospheres (Il’in & Voshchinnikov 1998). Needle-like iron dust has been also suggested to be present in the intergalactic space and to thermalize the cosmic microwave background radiation, possibly arising from the radiation of Population III stars (see Li 2003 and references therein). Note that in many cases the optical properties of iron grains were calculated in the Rayleigh approximation which however does not work for iron in the near-infrared because of its high refractive index. For example, at the wavelength $\lambda = 5 \mu\text{m}$, $m_{\text{Fe}} = 4.59 + 15.4i$ (Lynch & Hunter 1991) and the Rayleigh criterion $|m|x \ll 1$ is satisfied only for tiny particles ($r_s \ll 0.05 \mu\text{m}$).

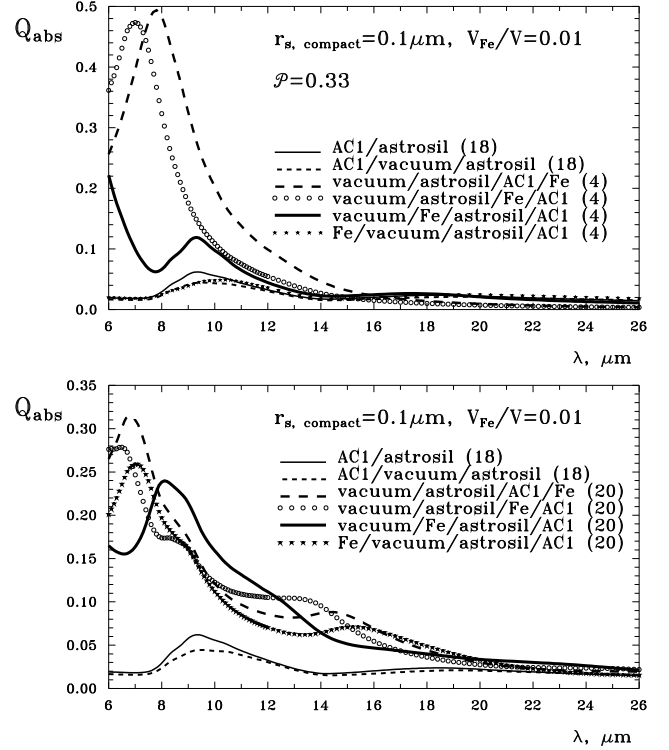


Fig. 21. Wavelength dependence of the absorption efficiency factors for multi-layered spheres of radius $r_{s, \text{compact}} = 0.1 \mu\text{m}$. Compact particles contain an equal fraction (50%) of AC1 and astrosil. Composite particles contain an equal fraction (33%) of AC1, astrosil and vacuum, the volume fraction of iron is 1%. All constituents are separated in equivolume layers. The cyclic order of the layers and their number are indicated.

In order to consider the influence of the metallic iron on the optical properties of multi-layered spheres we calculated the wavelength dependence of the absorption efficiency factors similar to what had been shown in Fig. 17. Some results are plotted in Fig. 21. In all cases the volume

fraction of iron was adopted to be equal to 1% of the total grain volume (or approximately 4% of grain mass). The iron was put in the form of one layer at different places inside the four-layered particle (Fig. 21, upper panel) or distributed as equivolume layers inside the 20-layered particle (Fig. 21, lower panel). As it can be seen, the presence of metallic iron at any place inside a particle, excluding its core, drastically changes the particle absorption. Iron totally screens the underlying layers and influences the optics of the overlying ones. The silicate features disappear and a very strong “pseudo-feature” with the centre between $6\ \mu\text{m}$ and $9\ \mu\text{m}$ arises instead of them. Such a feature was not observed in spectra of celestial objects, and hence definitive doubts appear that metallic iron is a noticeable component of dust grains, at least as a layer. However, iron can well form the core of a particle. Very likely, iron is oxidized in the result of redox reactions or is modified to sulfides (Duley 1980, Jones 1990).

9. Concluding remarks

We present a new model of composite grains which can be used for the interpretation of observations of interstellar, circumstellar and cometary dust. In our model the particles are represented by multi-layered spheres whose optical properties are calculated exactly. If the number of layers is small, the model obviously coincides with older models where the grains have several coatings. For a large ($\gtrsim 15 - 20$) number of the layers, the new model is shown to approximate heterogeneous particles consisting of several well mixed materials.

The model allows one a careful examination of the optical properties of very porous particles. Previously, this task was solved using the Mie theory for homogeneous spheres and effective refractive indices derived from different mixing rules of the Effective Medium Theory. We demonstrate that this approach gives wrong results when the porosity exceeds a value of 0.5. The application of a sophisticated layered-sphere mixing rule, recently suggested by Voshchinnikov & Mathis (1999), provides results of acceptable accuracy. Our study of the optics of porous grains allows us to conclude that a growth of porosity usually leads to:

- an increase of the extinction, scattering and absorption cross-sections (Figs. 8, 9);
- a growth of albedo (beginning with a size parameter value 2–3) and the asymmetry parameter (for particles of all sizes, Fig. 9);
- flattening of the wavelength dependence of extinction (Fig. 12);
- an increase of the sweeping efficiency for small particles and its decrease for large particles (Fig. 13);
- a growth of the intensity of radiation scattered in nearly forward directions and the transformation of the negative polarization to the positive one beginning with large scattering angles (Fig. 15);
- a decrease of grain temperature (Fig. 16);

- broadening of the infrared features and their shift to longer wavelengths (Fig. 17);
- a growth of the particle opacity in the mm domain (Table 1).

Note that some of our results contradict the previous calculations based on the approximate light scattering theory.

Application of our model to interpretation of the interstellar extinction and cosmic abundances observed in the direction of two stars shows that one can strongly reduce the model dust-phase abundances and hence partly resolve the carbon crisis. However, its final solution obviously needs more work on the model as well as better known reference cosmic abundances and their local variations.

We can also conclude that metallic iron hardly is a noticeable component of dust grains in the form of a layer because its presence at any place inside a particle drastically changes the particle absorption and leads to nonobserved phenomena (Fig. 21). An exception is if iron is located in the core.

Acknowledgements. We are thankful to Walter Wegner for the possibility to use unpublished data. The work was partly supported by grants of the Volkswagen Foundation (Germany), INTAS (Open Call 99/652), and the DFG Research Group “Laboratory Astrophysics”.

References

- Aden, A.L., & Kerker, M. 1951, *J. Appl. Phys.*, 22, 1242
- Allen, M.M., Snow, T.P., & Jenkins, E.B. 1990, *ApJ*, 355, 130
- Bohren, C.F., & Huffman, D.R. 1983, *Absorption and scattering of light by small particles*. John Wiley & Sons, New York
- Bouwman, J., de Koter, A., van den Ancker, M.E., & Waters, L.B.F.M. 2000, *AA*, 360, 213
- Bruggeman, D.A.G. 1935, *Ann. Phys.*, 24, 636
- Chlewicki, G., & Greenberg, J.M. 1984, *MNRAS*, 210, 791
- Chýlek, P., Videen, G., Geldart, D.J.W., Dobbie, J.S., & Tso, H.C.W. 2000, In *Light Scattering by Nonspherical Particles*, ed. M.I. Mishchenko et al., Academic Press, San Francisco, p. 274
- Clayton, G.C., Wolf, M.J., Sofia, U.J., Gordon, K.D., & Misselt, K.A. 2003, *astro-ph/0301488*
- Demyk, K., Jones, A.P., Dartois, E. Cox, P., & d’Hendecourt, L. 1999, *AA*, 349, 267
- Draine, B.T., & Lee, H.M. 1984, *ApJ*, 285, 89
- Duley, W.W. 1980, *ApJ*, 240, 950
- Duley, W.W., Jones, A.P., & Williams, D.A. 1989, *MNRAS*, 236, 709
- Farafonov, V.G. 2000, *Opt. Spectrosc.*, 88, 441
- Farafonov, V.G., Il’in, V.B., & Prokop’eva, M.S. 2003, *JQSRT*, in press
- Ferratori, A.S., & Gail, H.-P. 2001, *AA*, 371, 133
- Fitzpatrick, E.L. 1997, *ApJ*, 482, L199
- Fitzpatrick, E.L., & Massa, D.L. 1990, *ApJS*, 72, 163
- Gail, H.-P., & Sedlmayr, E. 1999, *AA*, 347, 594
- Garnett, J.C.M. 1904, *Phil. Trans. R. Soc.*, A 203, 385
- Greenberg, J.M. 1978, *Interstellar Dust*, In *Cosmic Dust*, ed. J.A.M. McDonnell, p. 187

- Greenberg, J.M. 1984, *Occas. Rep. Roy. Obs. Edinburgh*, N 12, 1
- Greenberg, J.M., & Hage, J.L. 1991, In *Chemistry in Space*, eds. J.M. Greenberg, & V. Pirronello, Kluwer, p. 363
- Greenberg, J.M., & Li, A. 1996, In *The Cosmic Dust Connection*, ed. J.M. Greenberg, Kluwer, p. 43
- Gurvich, I., Shiloah, N., & Kleiman, M. 2001, *JQSRT*, 70, 433
- Güttler, A. 1952, *Ann. Phys.*, 6, Bd. 11, 65
- Hage, J.L., & Greenberg, J.M. 1990, *ApJ*, 361, 251
- Harwit, M., Malfait, K., Decin, L. et al. 2001, *ApJ*, 557, 844
- Henning, Th. 1996, In *The Cosmic Dust Connection*, ed. J.M. Greenberg, Kluwer, p. 399
- Henning, Th., & Stognienko, R. 1993, *AA*, 280, 609
- Henning, Th., Il'in, V.B., Krivova, N.A., Michel, B., & Voshchinnikov, N.V. 1999, *AAS*, 136, 405
- Heney, L.G., & Greenstein, J.K. 1941, *ApJ*, 93, 70
- Hong, S.S., & Greenberg, J.M. 1980, *AA*, 88, 194
- Jäger, C., Il'in, V.B., Henning, Th., Mutschke, H., Fabian, D., Semenov, D.A., & Voshchinnikov, N.V. 2003, *JQSRT*, in press
- Johnson, B.R. 1996, *Appl. Opt.*, 35, 3286
- Jones, A.P. 1990, *MNRAS*, 245, 331
- Jones, A.P. 2000, *J. Geophys. Res.*, 105, 10257
- Jones, A.P., Duley, W.W., & Williams, D.A. 1990, *QJRAS*, 31, 567
- Iatì, M.A., Cecchi-Pestellini, C., Williams, D.A., Borghese, F., Denti, P., Saija, R., & Aiello, S. 2001, *MNRAS*, 322, 749
- Il'in, V.B., & Krivova, N.A. 2000, *Astron. Lett.*, 26, 379
- Il'in, V.B., & Voshchinnikov, N.V. 1998, *AAS*, 128, 187
- Kemper, F., de Koter, A., Waters, L.B.F.M., Bouwman, J., & Tielens, A.G.G.M. 2002, *AA*, 384, 585
- Kerker, M. 1969, *The Scattering of Light and Other Electromagnetic Radiation*. Academic Press, New York
- Kim, S.-H., Martin, P.G., & Hendry, P.D. 1994, *ApJ*, 422, 164
- Kimura, H., Okamoto, H., & Mukai, T. 2002, *Icarus*, 157, 349
- Knacke, R.F., Fajardo-Acosta, S.B., Tesco, C.M. Hackwell, J.A., Lynch, D.K., & Russel, R.W. 1993, *ApJ*, 418, 440
- Kolokolova, L., & Gustafson, B.Å.S. 2001, *JQSRT*, 70, 611
- Kozasa, T., Blum, J., & Mukai, T. 1992, *AA*, 263, 423
- Kozasa, T., Dorschner, J., Henning, Th., & Stognienko, R. 1996, *AA*, 307, 551
- Krügel, E., & Siebenmorgen, R. 1994, *AA*, 288, 929
- Laor, A., & Draine, B.T. 1993, *ApJ*, 402, 441
- Lewis, J.S., & Ney, E.P. 1979, *ApJ*, 234, 154
- Li, A. 2003, *ApJ*, 584, 593
- Li, A., & Greenberg, J.M. 1997, *AA*, 323, 566
- Li, A., & Greenberg J.M. 1998, *AA*, 331, 291
- Li, A., & Greenberg, J.M. 2002, *astro-ph/0204392*
- Lorenz-Martins, S., de Araújo, F.X., Codina Landaberry, S.J., de Almeida, W.G., & de Nader, R.V. 2001, *AA*, 367, 189
- Lynch, D.W., & Hunter, W.R. 1991, In *Handbook of Optical Constants of Solids II*, ed. E.D. Palik, Academic Press, New York, p. 385
- Mason, C.G., Gehr, R.D., Jones, T.J., Woodward, C.E., Hanner, M.S., & Williams, D.M. 2001, *ApJ*, 549, 635
- Mathis, J.S. 1996, *ApJ*, 472, 643
- Mathis, J.S., & Whiffen, G. 1989, *ApJ*, 341, 808
- Mathis, J.S., Rimpl, W., & Nordsieck, K.H. 1977, *ApJ*, 217, 425
- McCabe, E.M. 1982, *MNRAS*, 200, 71
- Ossenkopf, V., Henning, Th. 1994 *AA*, 291, 943
- Prishivalko, A.P., Babenko, V.A., & Kuz'min, V.N. 1984, *Scattering and Absorption of Light by Inhomogeneous and Anisotropic Spherical Particles*, Nauka i Tekhnika, Minsk
- Rouleau, F., & Martin, P.G. 1991, *ApJ*, 377, 526
- Savage, B.D., & Sembach, K.R. 1996, *ARAA*, 34, 279
- Serkowski, K., Mathewson, D.S., & Ford, V.L. 1975, *ApJ*, 196, 261
- Shifrin, K.S. 1952, *Izvestia Akademii Nauk SSSR, Ser. Geofizicheskaya*, N 2, 15
- Sihvola, A.H. 1999, *Electromagnetic Mixing Formulas and Applications*, Institute of Electrical Engineers, Electromagnetic Waves Series 47, London
- Snow, T.P., & Witt, A.N. 1996, *ApJ*, 468, L65
- Snow, T.P., Rachford, B.L., & Figoski, L. 2002, *ApJ*, 573, 662
- Spanier, J.E., & Herman, I.P. 2000, *Phys. Rev.*, B61, 10437
- Takei, Y., Fujimoto, R., Mitsuda, K., & Onaka, T. 2003, *astro-ph/0208290*
- Telesco, C.M., & Knacke, R.F. 1991, *ApJ*, 372, L29
- Vaidya, D.B., Gupta, R., Dobbie, J.S., & Chýlek, P. 2001, *AA*, 375, 584
- van de Hulst, H.C. 1957, *Light scattering by small particles*, John Wiley, New York
- Voshchinnikov, N.V. 2002, *Astrophys. & Space Phys. Rev.*, 12, 1
- Voshchinnikov, N.V., & Il'in, V.B. 1983, *SvA*, 27, 650
- Voshchinnikov, N.V., & Il'in, V.B. 1987, *SvAL*, 13, 157
- Voshchinnikov, N.V., & Mathis, J.S. 1999, *ApJ*, 526, 257 (VM)
- Wegner, W. 2002, private communication
- Weingartner, J.C., & Draine, B.T. 2001, *ApJ*, 548, 296
- Wickramasinghe, N.C. 1963, *MNRAS*, 126, 99
- Wiener, O. 1910, *Berichte über die Verhandlungen der Königlich-Sächsischen Gesellschaft der Wissenschaften zu Leipzig, Math.-phys. Klasse*, 62, 256
- Witt, A.N., & Gordon, K.D. 2000, *ApJ*, 528, 799
- Wolff, M.J., Clayton, G.C., Martin, P.G., & Schulte-Ladbeck, R.E. 1994, *ApJ*, 423, 412
- Wu, Z.S., & Wang, Y.P. 1991, *Radio Sci.*, 26, 1393
- Wu, Z.S., Guo, L.X., Ren, K.F., Gouesbet, G., & Gréhan, G. 1997, *Appl. Opt.*, 36, 5188
- Zubko, V.G., Krełowski, J., & Wegner, W. 1996, *MNRAS*, 283, 577